Electronic Supporting Information

Acid–Responsive Rhenium(I) NHC Complexes: Pyrazine vs Pyridine

Pedro O. Abate,[a, b, c, d] José Francisco Rizo,[a, b] Francisco José Fernández-de-Córdova,[b] Abel Ros,*[b] and Orestes Rivada-Wheelaghan[a,b]

a, Departamento de Química Inorgánica, Universidad de Sevilla, C/Prof. García González 1, 41012 Seville, Spain. E-mail: orivada@us.es

b, Instituto de Investigaciones Químicas, Centro de Innovación en Química Avanzada (ORFEO-CINQA), Consejo Superior de Investigaciones Científicas – Universidad de Sevilla, C/Américo Vespucio 49, 41092 Seville, Spain. E-mail: abel.ros@iiq.csic.es

c, Universidad de Buenos Aires, Facultad de Ciencias Exactas y Naturales, Departamento de Química Inorgánica, Analítica y Química Física, Pabellón 2, Ciudad Universitaria, C1428EHA, Buenos Aires, Argentina.

d, CONICET – Universidad de Buenos Aires. Instituto de Química-Física de Materiales, Ambientes y Energía (INQUIMAE), Pabellón 2, Ciudad Universitaria, C1428EHA, Buenos Aires, Argentina.

Table of Contents

1. General Information

1. Materials and methods.

General information and materials.

-Anhydrous dichloromethane and acetonitrile were obtained by distillation over CaH_2. Other solvents such as methanol, Et_2O, acetone and toluene were purchased in chromatographic purity and used as received. $[ReCl(CO)_5]$ was provided by Thermo and $Ag(CF_3SO_3)$ and Ag_2O by Alfa Aesa. The pyridine-derived azolium salt **X**[1] were and 2-(chloromethyl)pyrazine[2] synthesized following previously described procedures.

-All synthetic transformations were done in oven-dried Schlenk tubes under inert (Ar) atmosphere. T

-^{1}H and ^{13}C NMR spectra of the samples were measured in a Bruker Avance III 400 MHz equipment, operating at frequencies of 400.13 and 100.62 MHz for ^{1}H NMR and ^{13}C NMR, respectively using deuterated solvents with residual protons as internal references. ^{1}H, ^{13}C, and ^{15}N chemical shift assignments were performed by collecting 2D COSY, 2D ^{1}H-^{13}C HSQC, 2D ^{1}H-^{13}C HMBC, 2D ^{1}H-^{15}N-HMBC. Multiplicity of signals: s – singlet, d – doublet, t – triplet, q – quartet, br s – broad signal, m – multiplet.

-Low-temperature diffraction data were collected on a Bruker D8 Quest APEX-III single crystal diffractometer, equipped with a Photon III detector and a IμS 3.0 microfocus X-ray source. Data were collected by means of ω and φ scans using monochromatic radiation λ(Mo Kα1) = 0.71073 Å. The diffraction images collected were processed and scaled using APEX-4 v2021.4-0 software. The structures were solved with SHELXT and was refined against F2 on all data by full-matrix least squares with SHELXL,5 using Olex2 as graphical interface.6 All non-hydrogen atoms were refined anisotropically. Hydrogen atoms were included in the model at geometrically calculated positions and refined using a riding model, unless otherwise noted. The isotropic displacement parameters of all hydrogen atoms were fixed to 1.2 times the U value of the atoms to which they are linked (1.5 times for methyl groups).

---

[1] a) P. Pham, and C. Hilty, *Chem. Commun.*, 2020, **56**, 15466-15469. b) C. Cao, R. Sun, Q. Chen, L. Lv, Y. Shi, and G. Pang, *Transition Met. Chem.*, 2013, **38**, 351-358. c) A. K. Ressmann, M. Schneider, P. Gaertner, M. Weil, and K. Bica, *Monatshefte fur Chemie,* 2017, **148**, 139-148.

[2] Patent WO2018/67786, 2018, A1.

-High-resolution mass (HR-MS) determinations were performed at CRMPO on a Bruker MaXis 4G by ASAP (+ or -) or ESI and MALDI with CH_2Cl_2 as solvent techniques. Experimental and calculated masses are given with consideration of the mass of the electron.

-Absorption spectra in the UV-Vis region were recorded with a Hewlett-Packard 8453 diode array spectrometer (range 200–700 nm).

-IR spectra were measured in a FT-IR Bruker Tensor 27 spectrometer instrument.

-Elemental analyses were carried out at the Microanalytical Facility at IIQ, using a LECO TruSpec CHN analyzer for the determination of %C, %H, and %N with an estimated error of ±.

-Electrochemical measurements were performed under Ar with millimolar (mM) solutions of the compounds, an AUTOLAB (Metrohm) PGSTAT100N or PGSTAT204 potentiostat run with Nova 2.1.4 software. The electrolyte salt, tetrabutylammonium hexafluorophosphate ($[NBu_4][PF_6]$) for electrochemical analysis, was purchased from Sigma−Aldrich and a standard three-electrode arrangement consisting of a glassy carbon disc (surface area = 7.07 mm^2) as the working electrode, a platinum wire as the counter electrode and a reference electrode. The reference electrode was SCE. $[NBu_4][PF_6]$ for electrochemical and spectroelectrochemical measurements was recrystallized three times from ethanol and dried at 100°C under vacuum for 24 h before use. For cyclic voltammetry experiments, unless specified, a scan rate of 100 mV s^{-1} was employed. All potentials reported in this work are referenced to the SCE electrode. $E_{1/2}$ values were extracted from CV measurements as the averages between the anodic (Ea) and cathodic (Ec) peak potentials: $E_{1/2} = (E_a + E_c)/2$. The glassy carbon electrode was cleaned by following a two-step procedure, first polished with 1 μm diamond suspension, followed by polishing with 0.4 μm diamond suspension. The electrode was then sonicated in MilliQ water, rinsed with acetonitrile and air dried. UV-Vis spectra were recorded with a Honeycomb (Pine Research) spectroelectrochemical cell (optical pathlength 1.6 mm) with a Pt-patterned working and counter electrode and a Ag/AgCl (3M KCl) reference electrode. The electrochemical and UV-Vis spectroelectrochemical experiments were performed under Ar in acetonitrile $[Bu_4NPF_6]$ = 0.1 M solutions.

-DFT calculations were carried out with Gaussian-09 program package.[3] All molecules were optimized using the PBE1PBE hybrid functional.[4] The 6-311G(d,p) basis set was used for C, N, H, O and Cl atoms, while the LanL2DZ basis set, along with its pseudopotential was used for the Re atoms.[5] Dispersion interactions are taken into account with the Grimme dispersion correction with Becke-Johnson damping.[6] No symmetry restrictions were placed on the geometry optimizations and, depending on the spin multiplicity, restricted or unrestricted Kohn–Sham (UKS) approximations were taken into account. All optimized structures were confirmed as minima by analyzing the harmonic vibrational frequencies where no imaginary frequencies were found. To include solvent polarization effects, all the calculations were done by using the conductor-like polarizable continuum model (CPCM).[7] The contribution of different groups on the orbitals, electron density difference maps (EDDM), spin density plots (SD), calculated UV-Vis spectra and transitions related to them were obtained using the GaussSum Version 3.0 Program and plotted with Gauss View 6.31.[8] UV-Vis profiles were obtained by considering a typical half-bandwidth of $\Delta\nu_{1/2} = 3000$ cm^{-1} for all electronic transitions. (TD)DFT calculations were done by considering 100 states to simulate all UV-Vis spectra.

-Thin-layer chromatography (TLC) was performed on aluminum sheets precoated with Merck 5735 Kieselgel 60F254. Column chromatography was carried out with Merck 5735 Kieselgel 60F (0.040-0.063 mm mesh).

---

[3] M. J. Frisch, G. W. Trucks, H. B. Schlegel, G. E. Scuseria, M. A. Robb, J. R. Cheeseman, G. Scalmani, V. Barone, B. Mennucci, G. A. Petersson, H. Nakatsuji, M. Caricato, X. Li, H. P. Hratchian, A. F. Izmaylov, J. Bloino, G. Zheng, J. L. Sonnenberg, M. Hada, M. Ehara, K. Toyota, R. Fukuda, J. Hasegawa, M. Ishida, T. Nakajima, Y. Honda, O. Kitao, H. Nakai, T. Vreven, J. A. Montgomery, J. E. Peralta, F. Ogliaro, M. Bearpark, J. J. Heyd, E. Brothers, K. N. Kudin, V. N. Staroverov, T. Keith, R. Kobayashi, J. Normand, K. Raghavachari, A. Rendell, J. C. Burant, S. S. Iyengar, J. Tomasi, M. Cossi, N. Rega, J. M. Millam, M. Klene, J. E. Knox, J. B. Cross, V. Bakken, C. Adamo, J. Jaramillo, R. Gomperts, R. E. Stratmann, O. Yazyev, A. J. Austin, R. Cammi, C. Pomelli, J. W. Ochterski, R. L. Martin, K. Morokuma, V. G. Zakrzewski, G. A. Voth, P. Salvador, J. J. Dannenberg, S. Dapprich, A. D. Daniels, O. Farkas, J. B. Foresman, J. V. Ortiz, J. Cioslowski, and D. J. Fox, *Gaussian 09, Revision D.01*, Gaussian, Inc., Wallingford, CT, 2013.

[4] J. P. Perdew, K.Burke, and M. Ernzerhof, *Phys. Rev. Lett.* 1996, **77**, 3865-3868.

[5] a) A. D. Becke, *J Chem Phys* 1986, **84**, 4524-4529. b) A. D. Becke, *J Chem Phys* 1992, **96**, 2155-2160. c) C. Lee, W. Yang, and R. G. Parr, *Phys Rev B* 1988, **37**, 785-789.

[6] a) S. Grimme, S. Ehrlich, and L. Goerigk, *J. Comput. Chem.* 2011, **32**, 1456-1465. b) S. Grimme, J. Antony, S. Ehrlich, and H. Krieg, *J. Chem. Phys.* 2010, **132**, 154104.

[7] a) V. Barone, and M. Cossi, *J. Phys. Chem. A* 1998, **102**, 1995-2001. b) M. Cossi, N. Rega, G. Scalmani, and V. Barone *J. Comput. Chem.* 2003, **24**, 669-681.

[8] N. M. O'boyle, A. L. Tenderholt, and K. M. Langner, *J. Comp. Chem.* 2008, **29**, 839-845.

2. Synthesis of azolium salt $ClHL^{Pz}$.

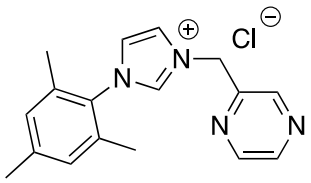

Over a Schlenk tube containing a solution of the mesitylimidazole (26 mmol) in 20 mL of anh. acetonitrile, freshly prepared 2-chloromethylpirazine (21.5 mmol, 2.76 g) was added. The resulting solution was stirred at 85 °C for 48h, cooled to rt, and the concentrated to dryness in the rotavap. The reaction crudes were purified by flash column chromatography using DCM/MeOH mixtures (DCM/MeOH 8:1→6:1) to afford **X** as a light brown foam (3.65 g, 54%). **^{1}H-RMN (500 MHz, $CDCl_3$, 298K):** δ 10.59 (s, 1H, $H_{imidazol}$), 9.11 (s, 1H, H_{Pyz}), 8.60 (d, *J* = 5 Hz, 1H, H_{Pyz}), 8.49 (s, 1H, H_{Pyz}), 7.98 (s, 1H, $H_{imidazol}$), 7.15 (s, 1H, $H_{imidazol}$), 6.99 (s, 2H), 6.36 (s, 2H, CH_2), 2.33 (s, 3H, CH_3), 2.06 (s, 6H, 2xCH_3).

^{13}C-RMN (125 MHz, $CDCl_3$, 298K): δ 148.9 (Cq), 145.3 (CH_{Pyz}), 145.2 (CH_{Pyz}), 144.3 (CH_{Pyz}), 141.5 (Cq), 139.4 (Cq), 134.4 ($CH_{imidazol}$), 130.8 (Cq), 130.0 (CH), 123.7 ($CH_{imidazol}$), 122.9 ($CH_{imidazol}$), 51.6 (CH_2), 21.2(CH_3), 17.7 (2xCH_3). **HRMS(ESI)** calculated for $C_{17}H_{19}N_4^+$ (M + Cl^-) 279.1604. Found 279.1606.

3. Synthesis of neutral Re-complexes complexes 1-2 and 3-4·X (X = OTf, BF_4 or PF_6).

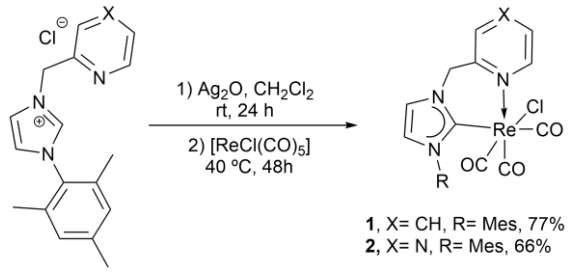

A dried Schlenk tube coated by aluminum foil was charged with the corresponding imidazolium salt **X-X** (0.5 mmol) and Ag_2O (0.55 mmol, 128 mg). After cycles of vacuum-N_2, anhydrous CH_2Cl_2 (16 mL) was added and the suspension was strongly stirred at rt for 24 hours. Then, the reaction crude was filtered through celite, washed with CH_2Cl_2, and concentrated in the rotavap to give the silver carbene in quantitative yield. The silver carbene was dissolved in anhydrous CH_2Cl_2 (16 mL), transferred via cannula to a Schlenk tube containing the [$ReCl(CO)_5$] (0.55 mmol,

199 mg) and the resulting solution was stirred on dark at 40 °C for 48 hours. Then, the solvent was evaporated and the reaction crude purified by flash column chromatography (CH_2Cl_2/acetone mixtures).

Synthesis of **1**.

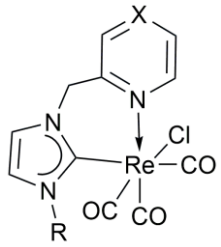

1, X= CH, R= Mes

Following the general procedure (0.5 mmol scale), purification by column chromatography (DCM/acetone 10:1) afforded **1** as a white solid (226 mg, 77%). **^{1}H-RMN (400 MHz, DMSO-d$_6$, 298K):** δ 9.09 (d, *J* = 8.0 Hz, 1H, H_1), 8.16 (t, *J* = 8.0 Hz, 1H, H_3), 7.83 (d, *J* = 8.0 Hz, 1H, H_4), 7.78 (s, 1H, H_5), 7.56 (t, *J* = 8.0 Hz, 1H, H_2), 7.40 (s, 1H, H_5), 7.02 (d, *J* = 5.5 Hz, 2H, $H_{imidazol}$), 6.17 (d, *J* = 12.0 Hz, 1H, CH_2), 5.37 (d, *J* = 12.0 Hz, 1H, CH_2), 2.31 (s, 3H, CH_3), 2.05 (s, 3H, CH_3), 1.94 (s, 3H, CH_3).**^{13}C-RMN (100 MHz, DMSO-d$_6$, 298K):** δ 197.4 (CO), 196.1 (CO), 192.6 (CO), 182.8 (C_{NHC}), 158.6 (C_1), 155.8, 140.8 (C_3), 138.7, 136.5, 136.3, 135.6, 129.4 ($C_{imidazol}$), 129.0 ($C_{imidazol}$), 126.5 (C_4), 125.9 (C_2), 123.4 (C_5), 123.4 (C_5), 55.0 (CH_2), 21.1 (CH_3), 18.6 (CH_3), 18.1 (CH_3). **HRMS(ESI)** calculated for $C_{21}H_{19}O_3N_3ClNaRe$ ($M + Na^+$) 606.0565. Found 606.0556. **Elemental analysis:** Teo.: 43.11% C, 3.62% H, 7.18% N. Exp.: 43.58% C, 3.66% H, 6.91% N. **IR for CO bands (cm^{-1}):** 1865, 1908, 2010.

Synthesis of **2**.

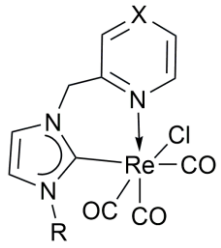

2, X= N, R= Mes

Following the general procedure (0.6 mmol scale), purification by column chromatography (DCM/acetone 10:1) afforded **2** as a white solid (280 mg, 80%). X-ray quality crystals were obtained by slow diffusion of toluene in a CH_2Cl_2 solution of **X**. **^{1}H-RMN (400 MHz, CD_2Cl_2, 298K):** δ 9.12 (d, *J* = 3.2 Hz, 1H, H_1), 8.87 (s, 1H, H_3), 8.62 (d, *J* = 3.2 Hz, 1H, H_2), 7.34 (d, *J* = 4.0 Hz, 1H, $H_{Imidazol}$), 7.02 (s, 2H, H_4), 6.97 (d, *J* = 4.0 Hz, 1H, $H_{Imidazol}$), 6.23 (d, *J* = 15.4 Hz, 1H, CH_2), 5.27 (d, *J* = 15.4 Hz, 1H, CH_2), 2.36 (s, 3H, CH_3), 2.11 (s, 3H, CH_3), 2.02 (s, 3H, CH_3). **^{13}C-RMN (100 MHz, CD_2Cl_2, 298K):** δ 195.8 (CO), 194.9 (CO), 191.3 (CO), 183.8 (C_{NHC}), 151.7 (C_1), 150.3, 146.4 (C_2), 146.1 (C_3), 139.5, 136.6, 135.5, 129.3 (C_4), 128.9 (C_4), 122.9 ($C_{Imidazol}$), 122.1 ($C_{Imidazol}$), 53.0 (CH_2), 20.9 (CH_3), 18.2 (CH_3), 17.8 (CH_3). **HRMS(ESI)** calculated for $C_{20}H_{18}N_4O_3Re$ ($M - Cl^-$) 549.0931. Found 549.0934.

Elemental analysis: Teo.: 40.99% C, 3.44% H, 9.56% N. Exp.: 41.38% C, 3.38% H, 9.42% N. **IR for CO bands (cm^{-1}):** 1875, 1910, 2012.

4. Synthesis of cationic Re-complexes 3-4.

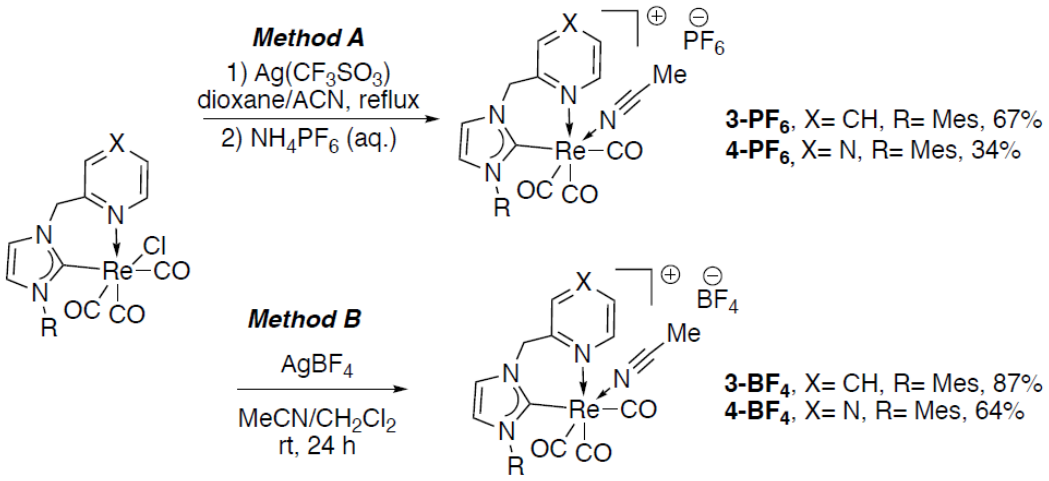

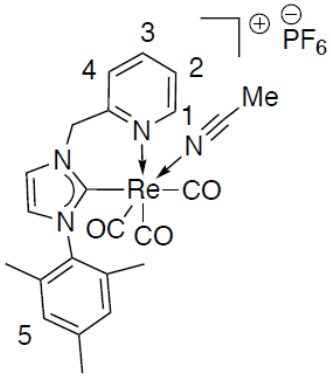

[Re(CO)3(NHC-py)(CH3CN)] **3-PF6:** 100 mg (0.172 mmol) of **1** was suspended in 30 mL of Ar-degassed 1,4-Dioxane in a 50 mL two-neck round bottom flask. The suspension was protected from light and 42.6 mg (0.166 mmol) of $Ag(CF_3SO_3)$ were added under Ar. The mixture was refluxed at 80 °C for 2 h under. After this time, 5 mL of degassed CH_3CN was added and the refluxed for an additional 3h. Upon cooling to r.t., the mixture was kept at 5° C for 2 h, the suspension was filtered to put aside the formed AgCl and the solvent was rotoevaporated to 1 mL. The remaining solution was added dropwise to 3 mL of a saturated NH_4PF_6 aqueous solution. The mixture was kept at 5 C for two days and the formed solid was collected on a frit, washed with cold H_2O (2 x 10 mL), Et_2O (2 x 10 mL) and dried under vacuum afforded **3** as a colorless solid. Yield: 85 mg (67%). Suitable crystals for XRD were growth by slow evaporation of a DCM/MeCN/Toluene (1/1/2) mixture. **^{1}H-RMN (400 MHz, CD_2Cl_2, 298K):** δ 8.97 (d, *J* = 8.0 Hz, 1H, H_1), 8.07 (t, *J* = 8.0 Hz, 1H, H_3), 7.85 (d, *J* = 8.0 Hz, 1H, H_4), 7.58 (s, 1H, H_5), 7.51 (t, *J* = 8.0 Hz, 1H, H_2), 7.07 (s, 1H, H_5), 7.03 (d, *J* = 5.5 Hz, 2H, $H_{imidazol}$), 5.58 (d, *J* = 12.0 Hz, 1H, CH_2), 5.42 (d, *J* = 12.0 Hz, 1H, CH_2), 2.37 (s, 3H, CH_3, MeCN) , 2.34 (s, 3H, CH_3), 2.04 (s, 3H, CH_3), 1.96 (s, 3H, CH_3).**^{13}C-RMN (100 MHz, CD_2Cl_2,**

298K): δ 192.8 (CO), 191.9 (CO), 191.3 (CO), 178.8 (C_{NHC}), 157.7 (C_1), 155.3, 140.8 (C_3), 140.1, 136.1, 136.3, 135.1, 134.9, 129.7 ($C_{imidazol}$), 128.9 ($C_{imidazol}$), 126.8, 126.2 (C_4), 123.6 (C_2), 123.3 (C_5), 122.8 (C_5), 56.2 (CH_2), 20.9 (CH_3), 17.8 (CH_3), 17.6 (CH_3), 3.7 (CH_3CN). **Elemental analysis** for $ReC_{23}N_4O_3H_{22}PF_6$ Teo.: 37.66% C, 3.02% H, 7.64% N. Exp.: 37.93% C, 2.74% H, 7,37% N. **IR (CH_3CN)**, ν_{CO} (cm^{-1}): 2033, 1933, 1923.

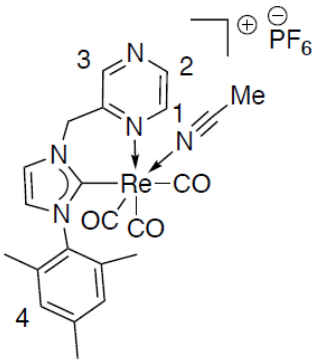

[Re(CO)$_3$(NHC-pz)(CH$_3$CN)] **4-PF$_6$:** 100 mg (0.171 mmol) of **2** were dissolved in 50 mL of argon-degassed, anhydrous acetonitrile (CH_3CN) in a 100 mL two-neck round-bottom flask. The suspension was protected from light, and 41.1 mg (0.162 mmol) of $AgPF_6$ were added under an argon atmosphere. The reaction mixture was stirred at room temperature in the dark for 7 days. After this period, the mixture was filtered to remove the precipitated AgCl and concentrated to ~2 mL under reduced pressure. The addition of 50 mL of diethyl ether (Et_2O) followed by storage at –15 °C yielded **4** as a pale yellow solid, which was isolated by filtration. Yield: 45 mg (34%). Suitable crystals for XRD were growth by slow evaporation of a DCM/MeCN/Toluene (1/1/2) mixture. **^{1}H-RMN (400 MHz, CD_2Cl_2, 298K):** δ 9.16 (s, 1H, H_3), 8.94 (d, *J* = 3.2 Hz, 1H, H_1), 8.74 (d, *J* = 3.2 Hz, 1H, H_2), 7.73 (s, 1H, $H_{Imidazol}$), 7.06 (s, 2H, H_4), 7.03 (s, 1H, $H_{imidazol}$), 5.81 (d, *J* = 16.4 Hz, 1H, CH_2), 5.49 (d, *J* = 16.4 Hz, 1H, CH_2), 2.39 (s, 3H, CH_3), 2.37 (s, 3H, CH_3CN), 2.02 (s, 3H, CH_3), 1.98 (s, 3H, CH_3). **^{13}C-RMN (100 MHz, CD_2Cl_2, 298K):** δ 192.1 (CO), 191.0 (CO), 190.8 (CO), 177.9 (C_{NHC}), 150.7 (C_{Pyz}), 150.1, 147.8 (C_{Pyz}), 147.4 (C_{Pyz}), 140.2, 135.9, 135.1, 129.7 (C_4), 129.0 (C_4), 124.0 ($C_{Imidazol}$), 123.5 ($C_{Imidazol}$), 54.0 (CH_2), 20.9 (CH_3), 17.8 (CH_3), 17.6 (CH_3), 3.8 (CH_3CN). **Elemental analysis** for $ReC_{22}N_5O_3H_{21}PF_6$ Teo.: 35.97% C, 2.88% H, 9.53% N. Exp.: 36.21% C, 2.52% H, 9.21% N. **IR (CH_3CN)**, ν_{CO} (cm^{-1}): 2035, 1938, 1926.

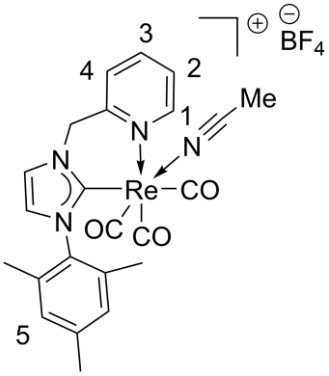

[Re(CO)$_3$(NHC-py)(CH$_3$CN)] **3-BF$_4$:** Inside a glovebox, a dried Schlenk tube coated by aluminium foil was charged with the corresponding Re complex **1** (0.2 mmol, 117 mg) and $AgBF_4$ (0.22 mmol, 43 mg). Then, a 1:3 mixture of anhydrous $MeCN/CH_2Cl_2$ (8 mL) was added and the reaction was stirred in dark at rt for 24 hours. Then, the reaction was concentrated to dryness, dissolved in CH_2Cl_2 and filtered through celite. The solvent was evaporated to give a yellow solid which was crystallized from a CH_2Cl_2/Et_2O mixture to afford *[Re(CO)$_3$(NHC-py)(CH$_3$CN)]* **(3)BF$_4$** (125 mg, 87%). The ^1H and ^{13}C-NMR spectra matched with **3-PF$_6$.**

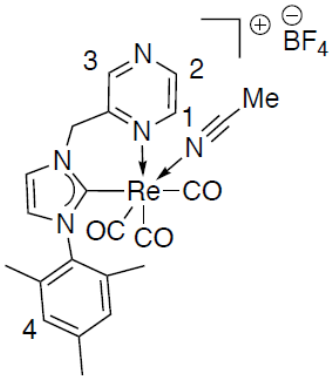

[Re(CO)$_3$(NHC-pz)(CH$_3$CN)] **4-BF$_4$:** Inside a glovebox, a dried Schlenk tube coated by aluminium foil was charged with the corresponding Re complex **2** (0.2 mmol, 117 mg) and $AgBF_4$ (0.22 mmol, 43 mg). Then, a 1:3 mixture of anhydrous $MeCN/CH_2Cl_2$ (8 mL) was added and the reaction was stirred in dark at rt for 24 hours. Then, the reaction was concentrated to dryness, dissolved in CH_2Cl_2 and filtered through celite. The solvent was evaporated to give a yellow solid which was crystallized from a CH_2Cl_2/Et_2O mixture to afford *[Re(CO)$_3$(NHC-pz)(CH$_3$CN)]* **4-BF$_4$** (92 mg, 64%). The ^1H and ^{13}C-NMR spectra matched with **4-PF$_6$.**

5. NMR, IR and HRMS spectra.

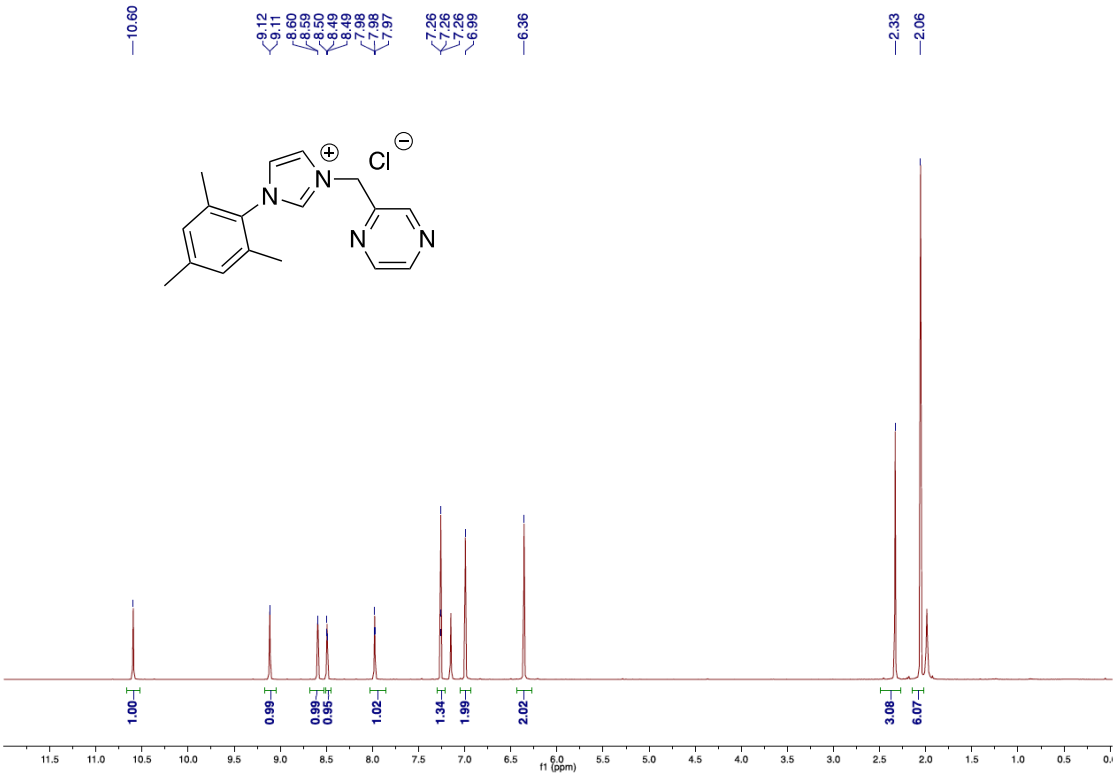

Figure S1. 500 MHz ^{1}H-NMR spectrum of **ClHL^{Pz}** dissolved in $CDCl_3$ at 298K.

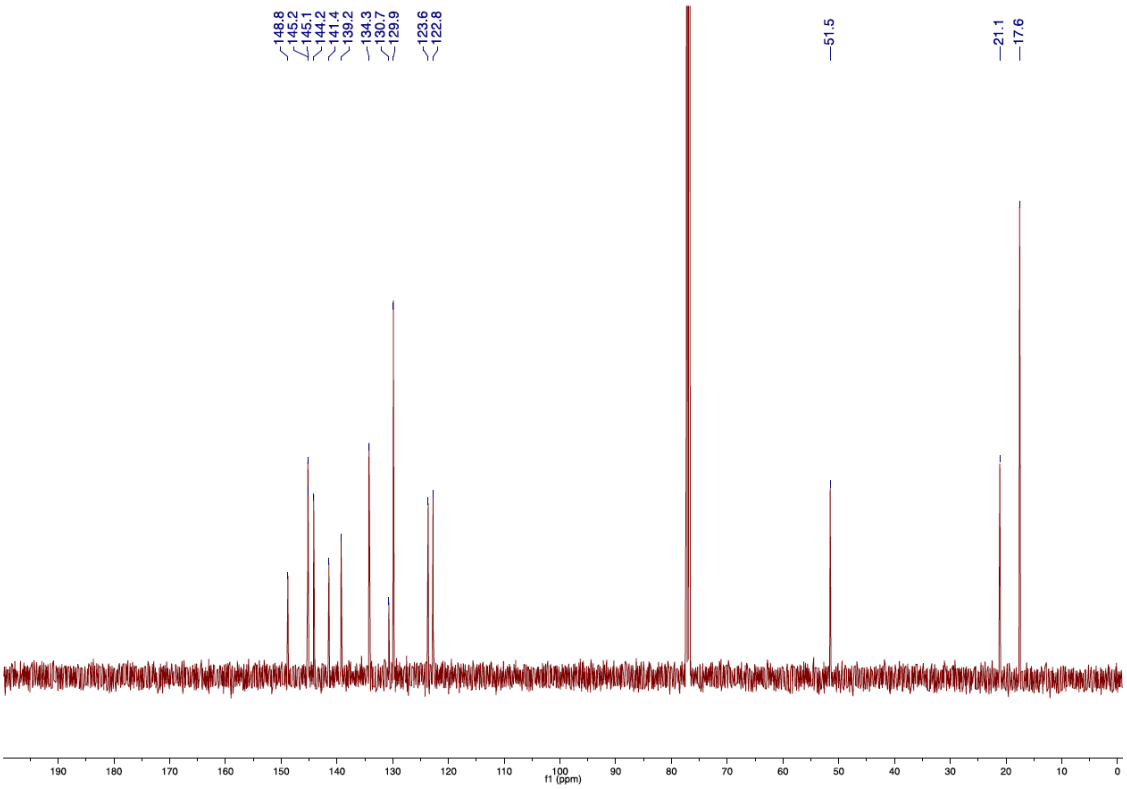

Figure S2. 125 MHz ^{1}H-NMR spectrum of **ClHL^{Pz}** dissolved in $CDCl_3$ at 298K.

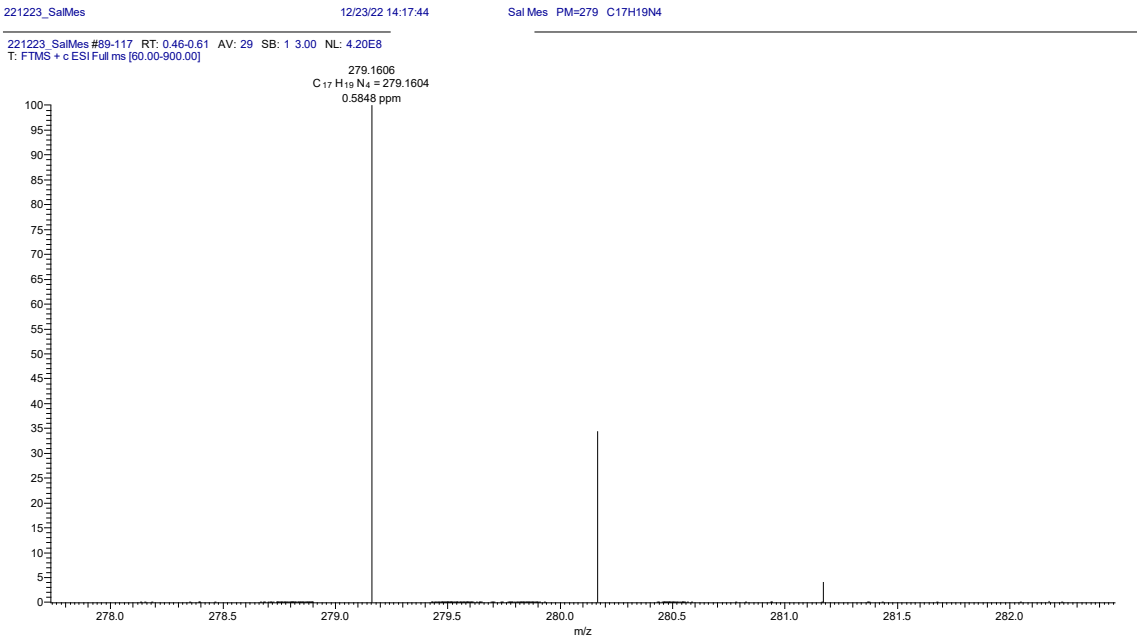

Figure S3. HRMS-ESI for **ClHL^{Pz}**.

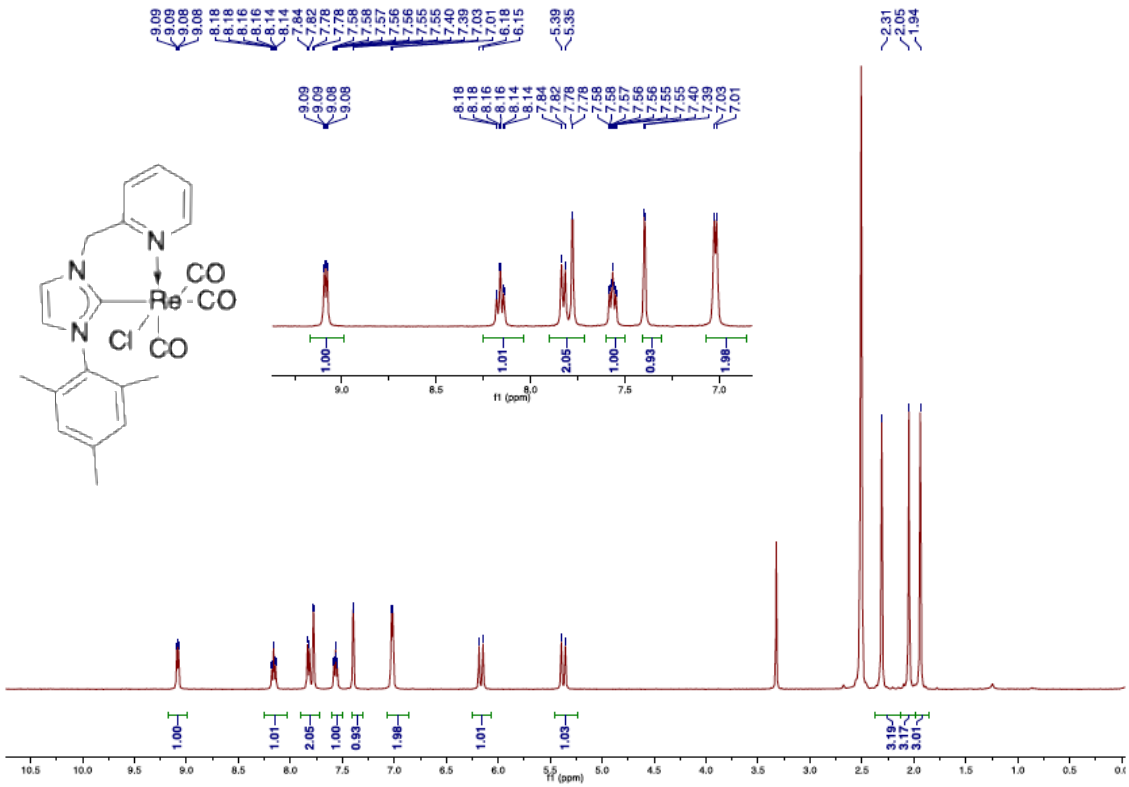

Figure S4. 400 MHz ^{1}H-NMR spectrum of **1** dissolved in DMSO-d_6 at 298K.

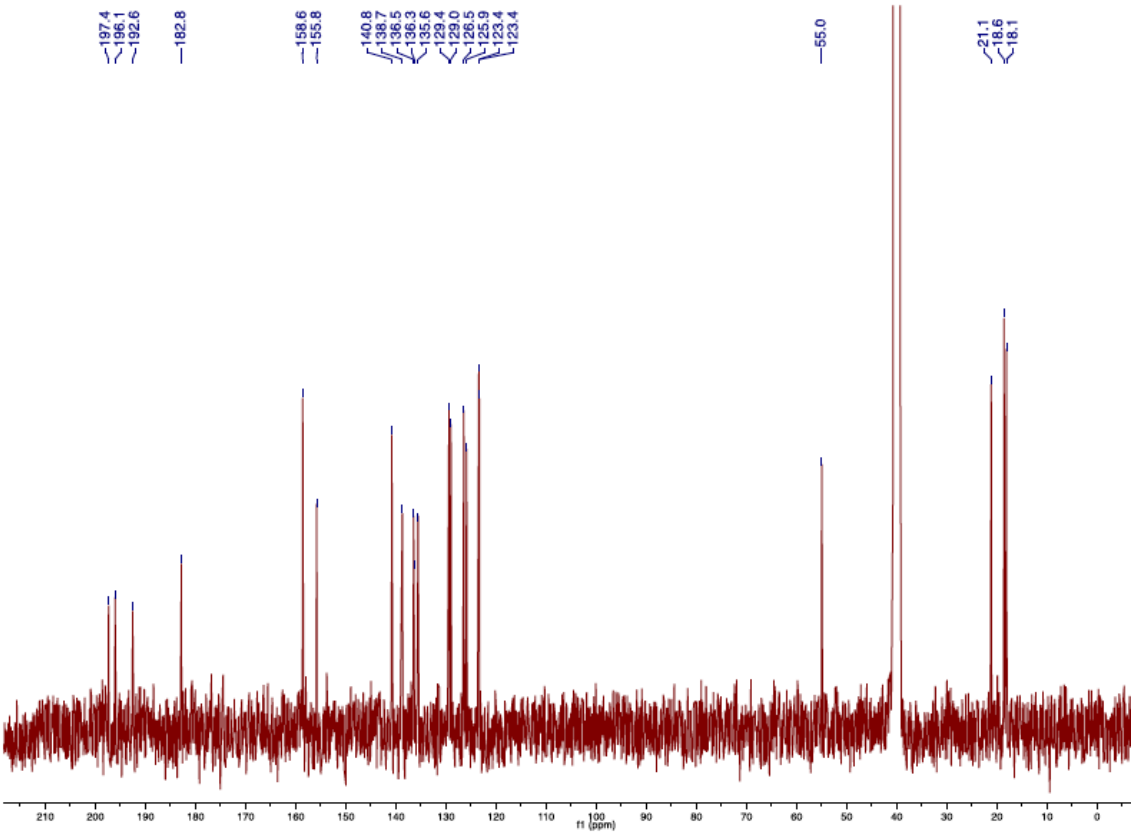

Figure S5. 100 MHz ^{13}C-NMR spectrum of **1** dissolved in DMSO-d_6 at 298K.

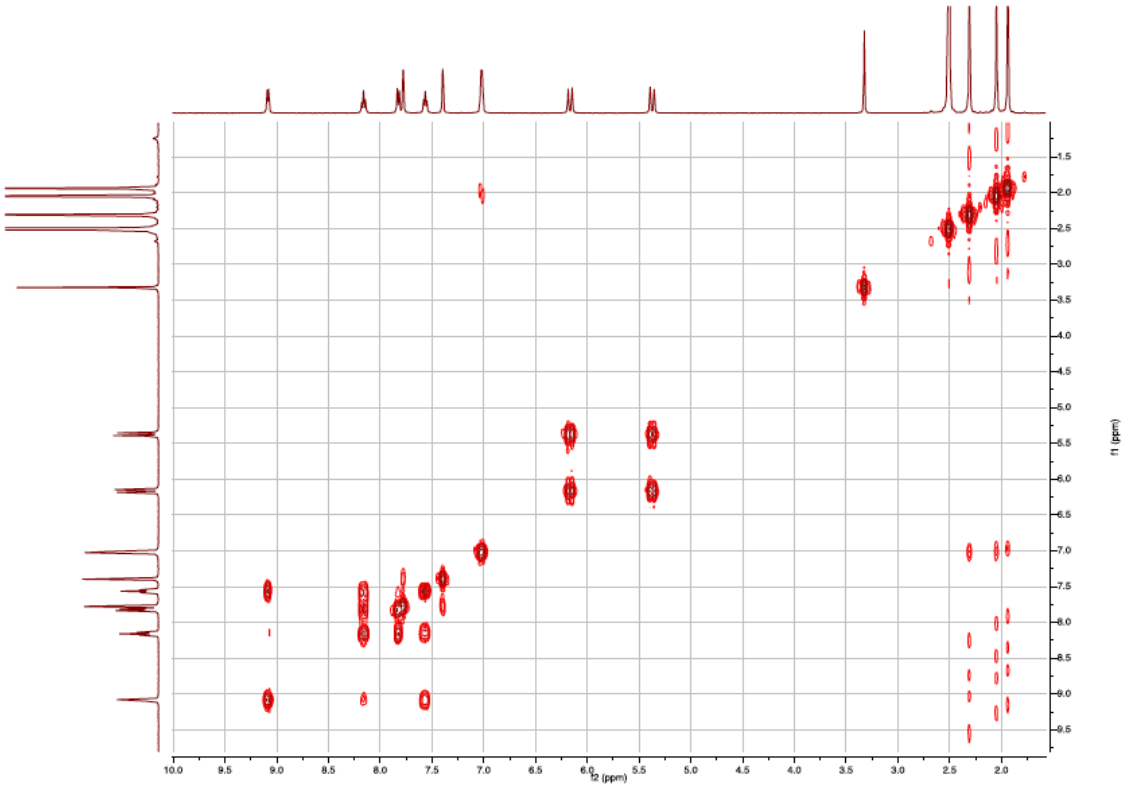

Figure S6. ^{1}H-^{1}H COSY spectrum of **1** dissolved in DMSO-d_6 at 298K.

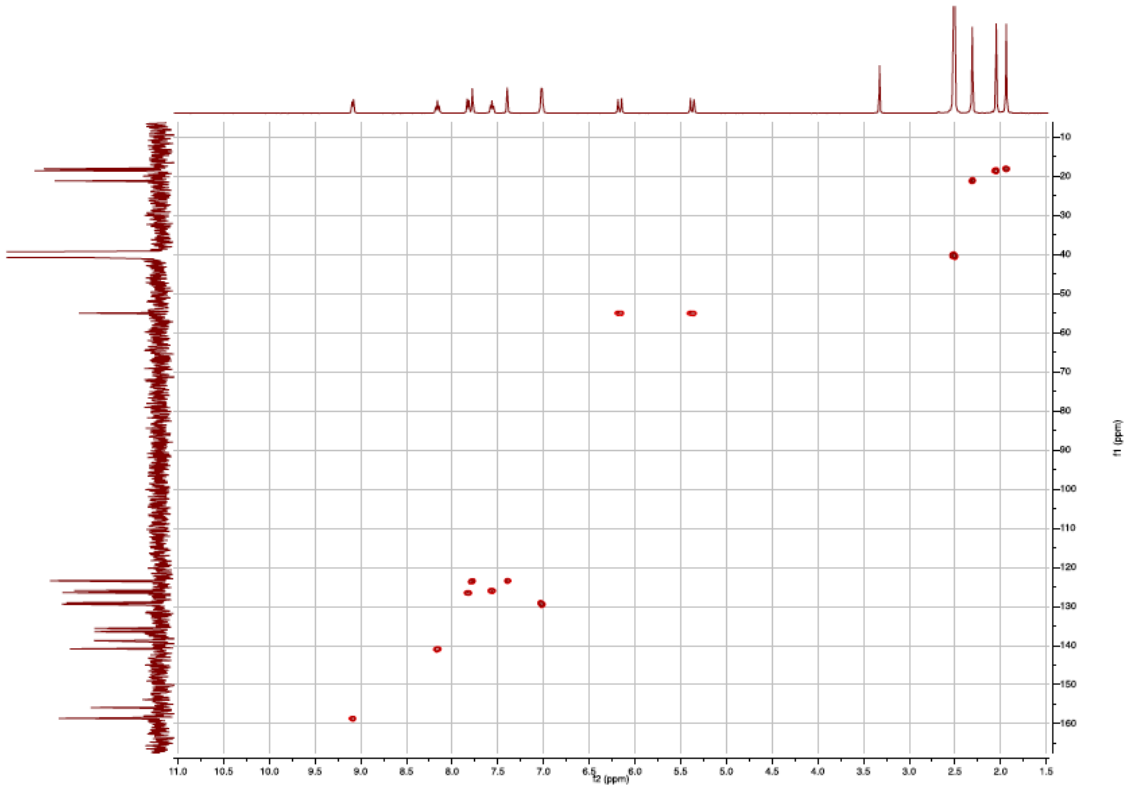

Figure S7. ^{1}H-^{13}C HSQC spectrum of **1** dissolved in DMSO-d_6 at 298K.

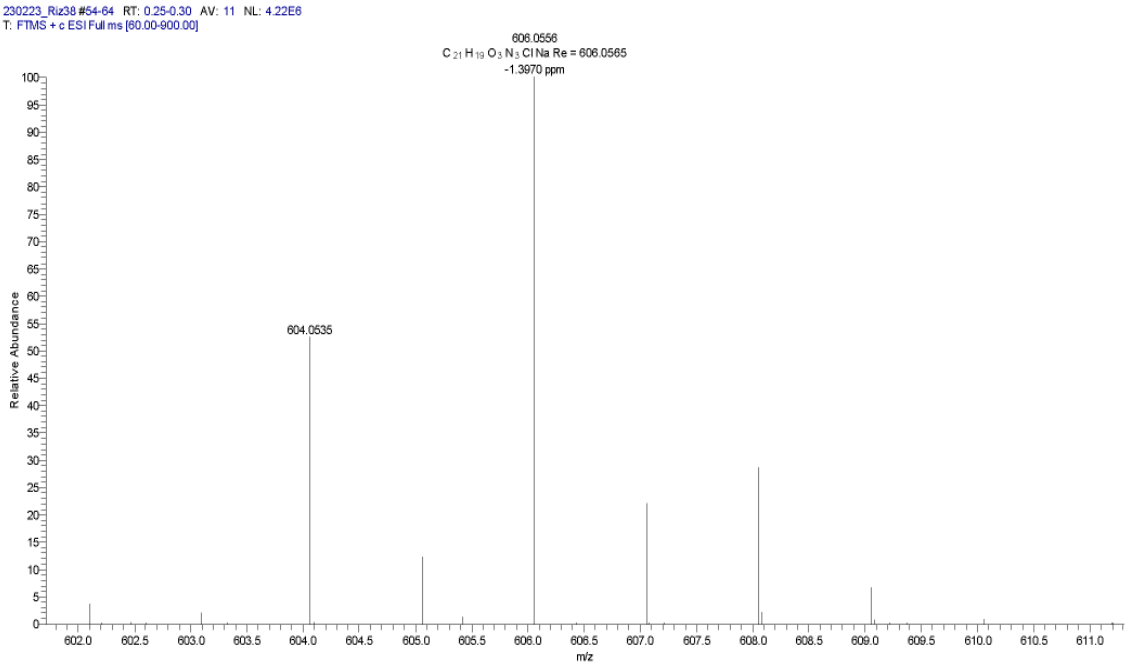

Figure S8. HRMS-ESI for **1**.

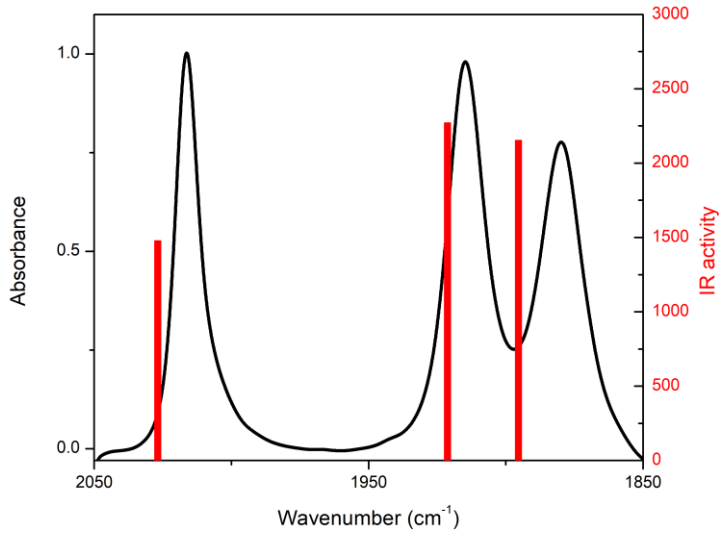

Figure S9. IR spectra of **1** in acetonitrile (black line). DFT calculated frequencies (red vertical bars)

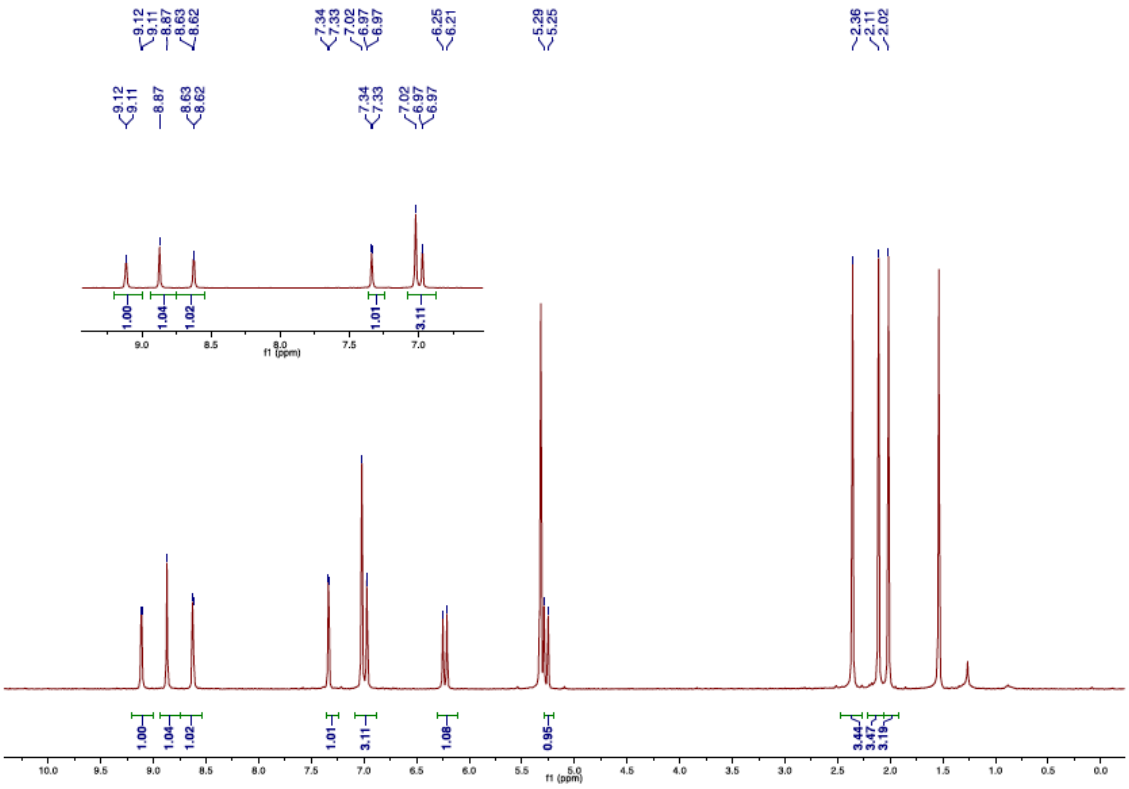

Figure S10. 400 MHz ^{1}H-NMR spectrum of **2** dissolved in CD_2Cl_2 at 298K.

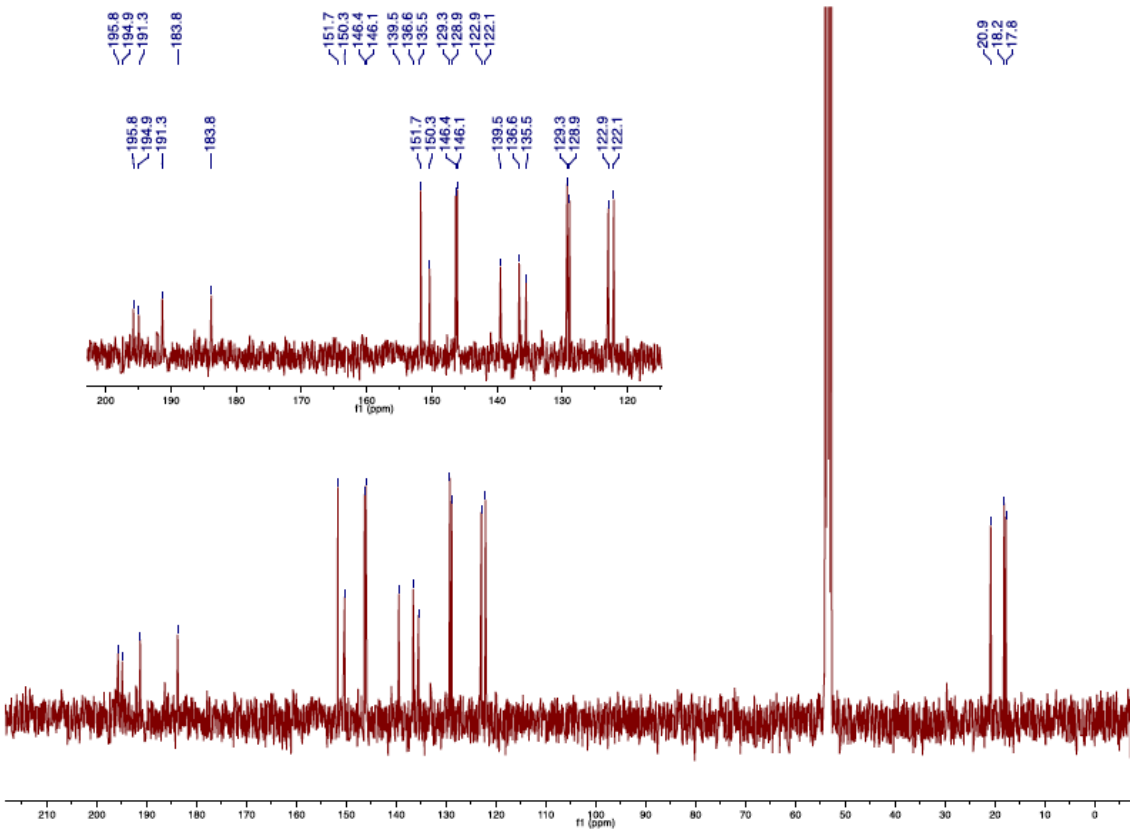

Figure S11. 100 MHz ^{13}C-NMR spectrum of **2** dissolved in CD_2Cl_2 at 298K.

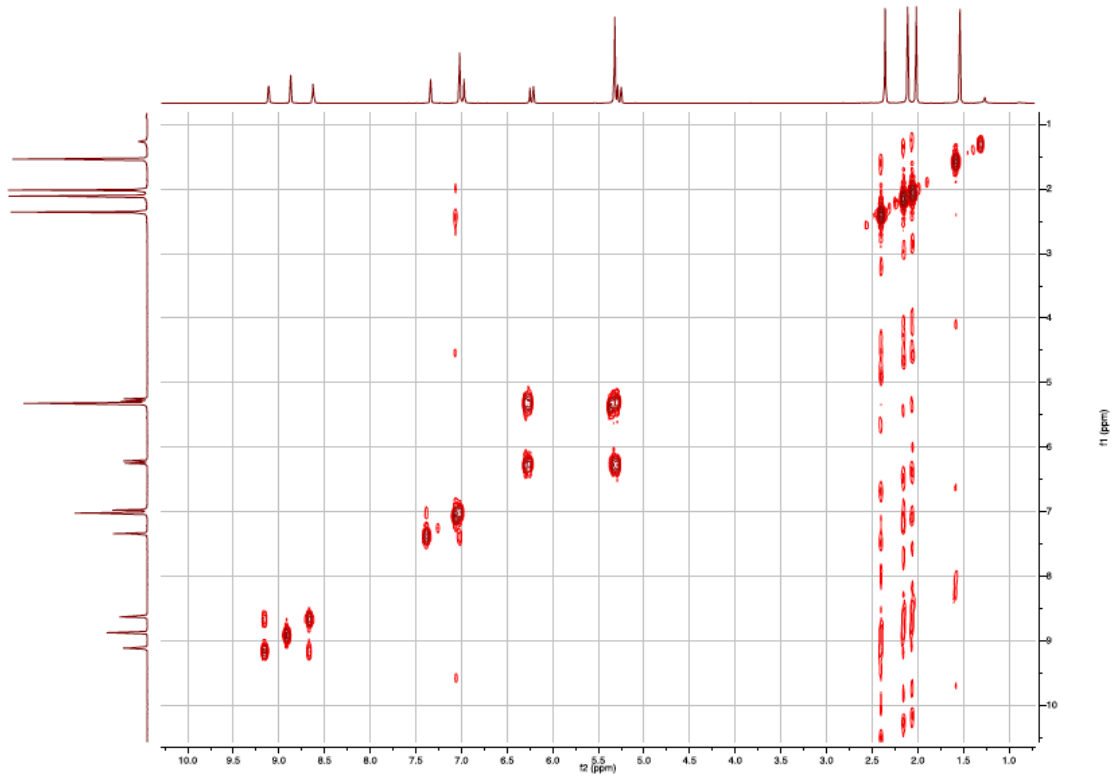

Figure S12. ^{1}H-^{1}H COSY spectrum of **2** dissolved in CD_2Cl_2 at 298K.

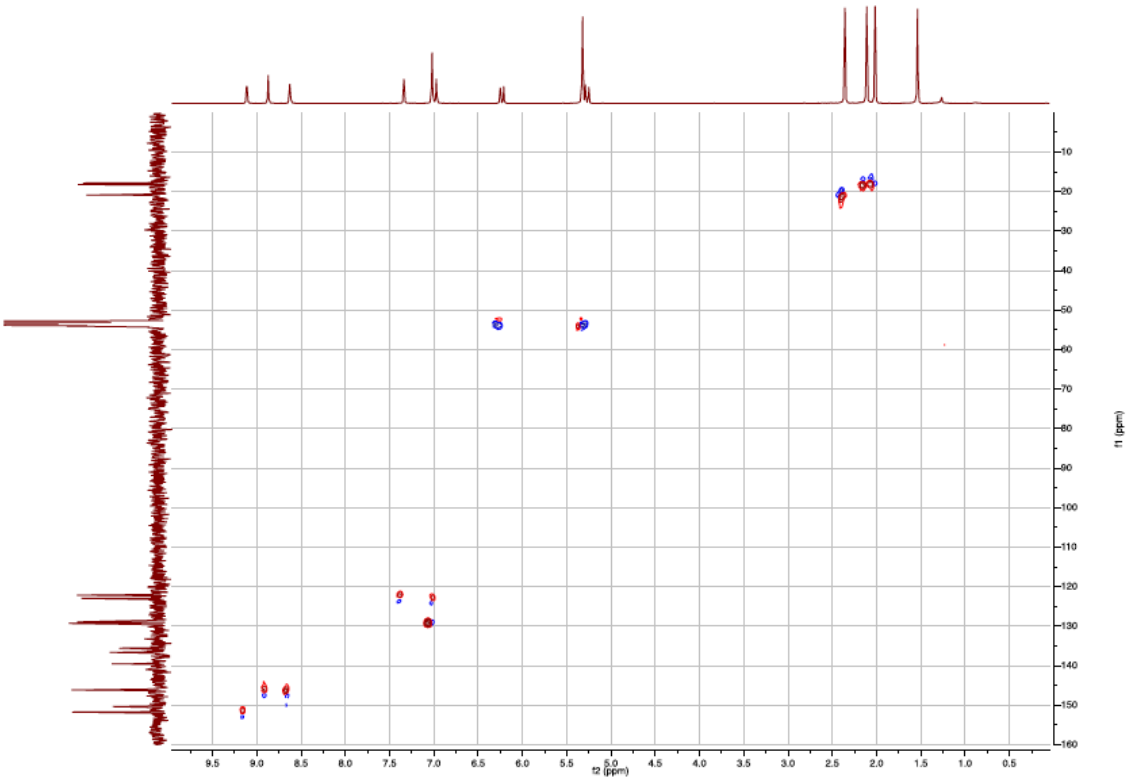

Figure S13. ^{1}H-^{13}C HSQC spectrum of **2** dissolved in CD_2Cl_2 at 298K.

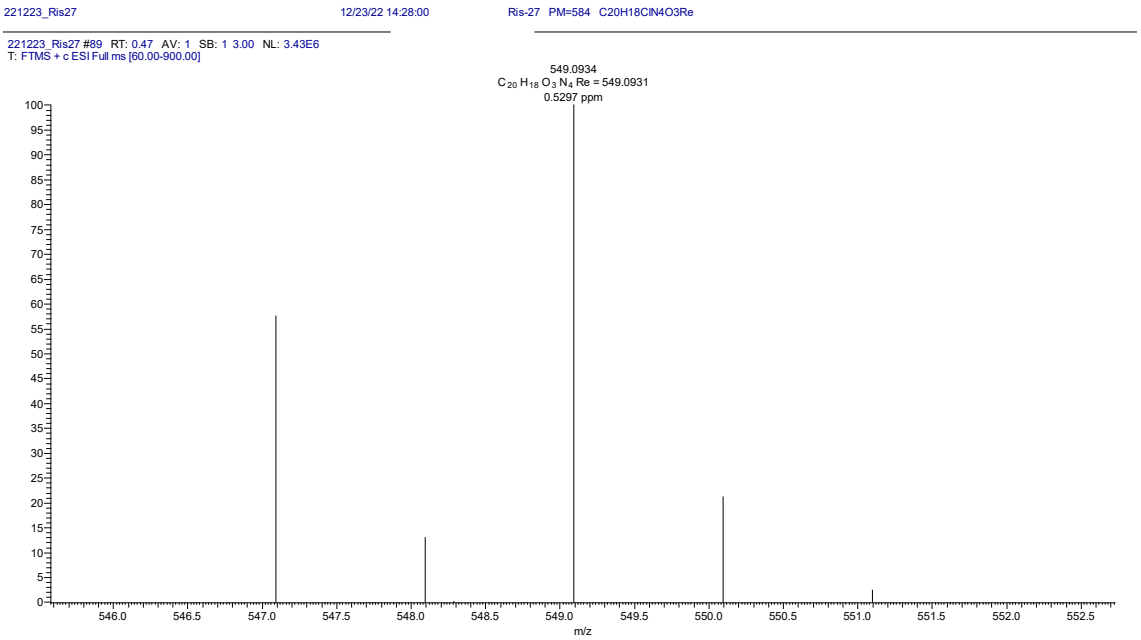

Figure S14. HRMS-ESI for **2**.

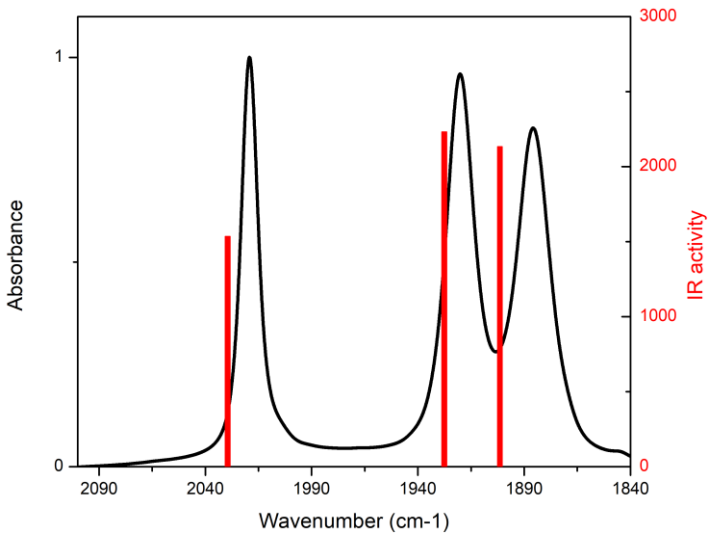

Figure S15. IR spectra of **2** in acetonitrile (black line). DFT calculated frequencies (red vertical bars).

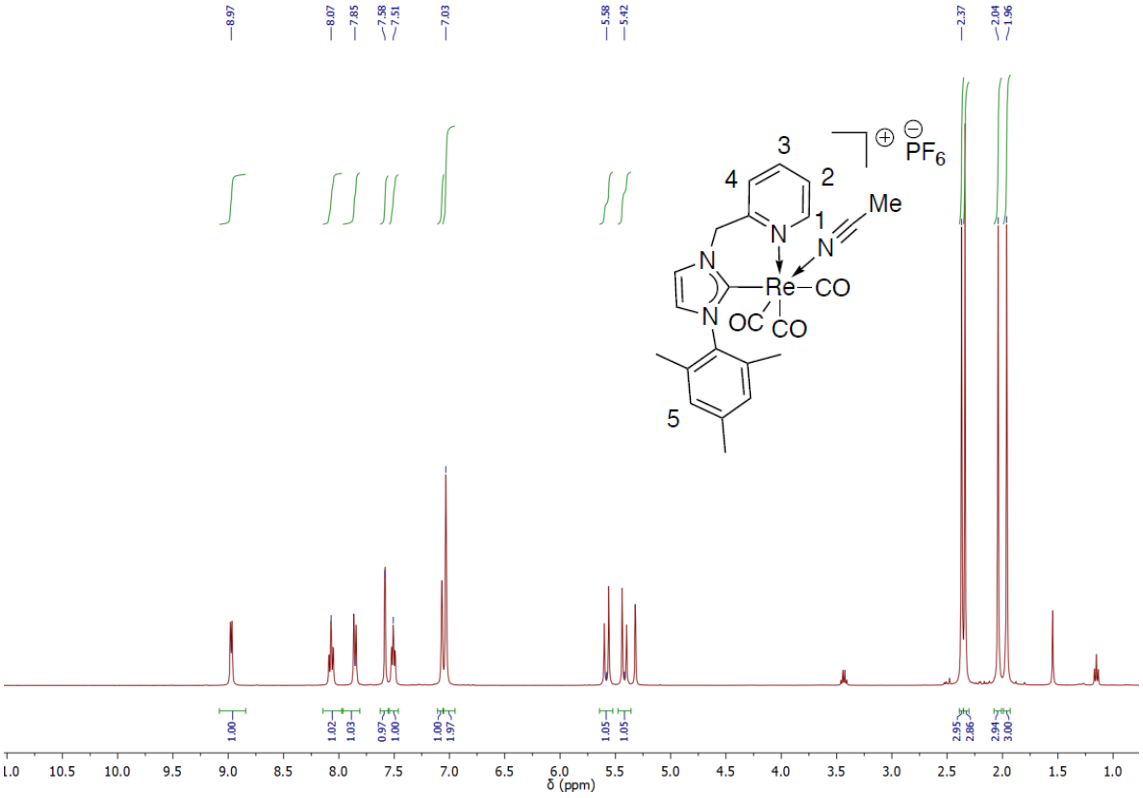

Figure S16. 400 MHz ^{1}H-NMR spectrum of **3·PF$_6$** dissolved in CD_2Cl_2 at 298K.

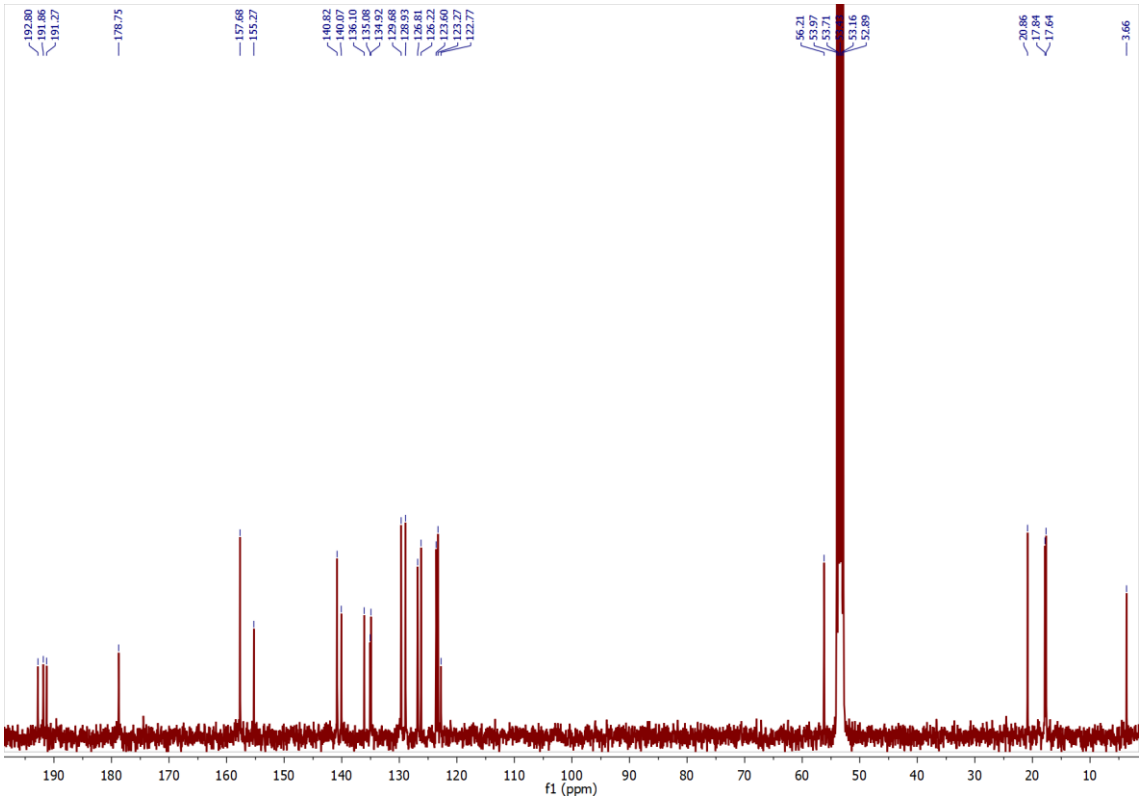

Figure S17. 100 MHz ^{1}H-NMR spectrum of **3·PF$_6$** dissolved in CD_2Cl_2 at 298K.

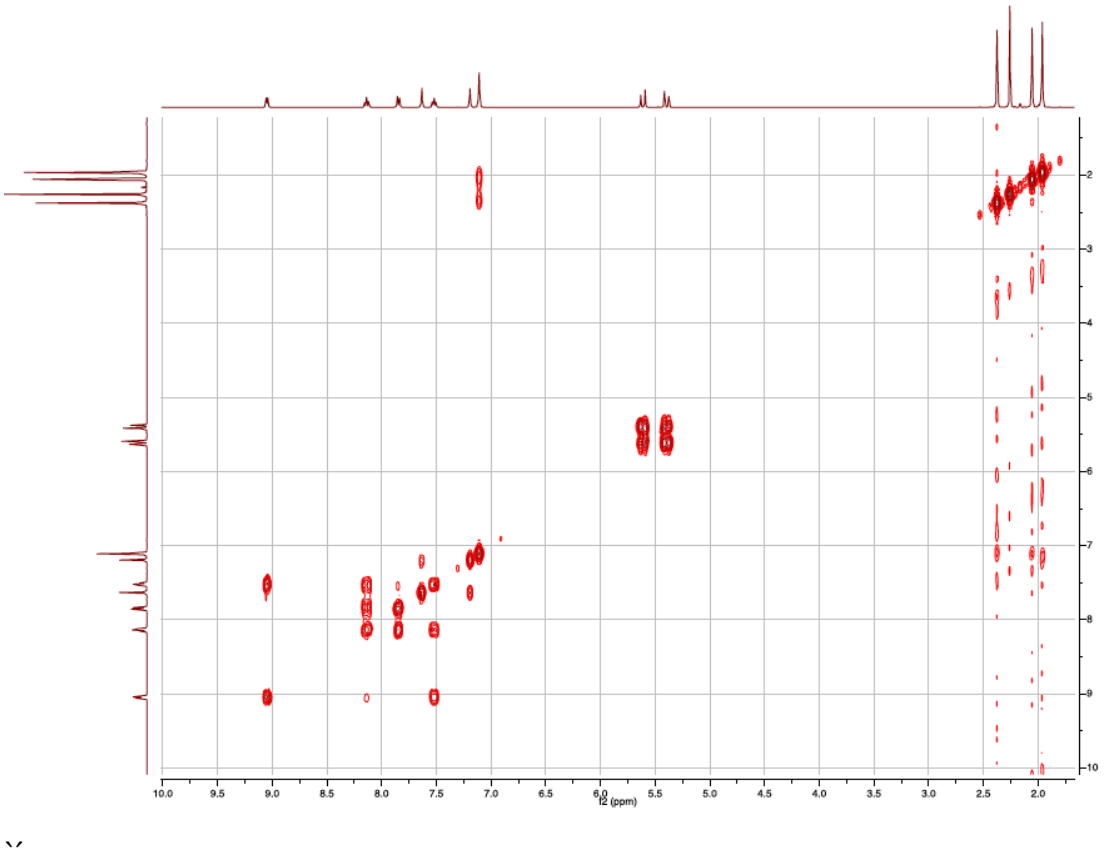

Figure S18. ^{1}H-^{1}H COSY spectrum of **3·PF$_6$** dissolved in CD_3CN at 298K.

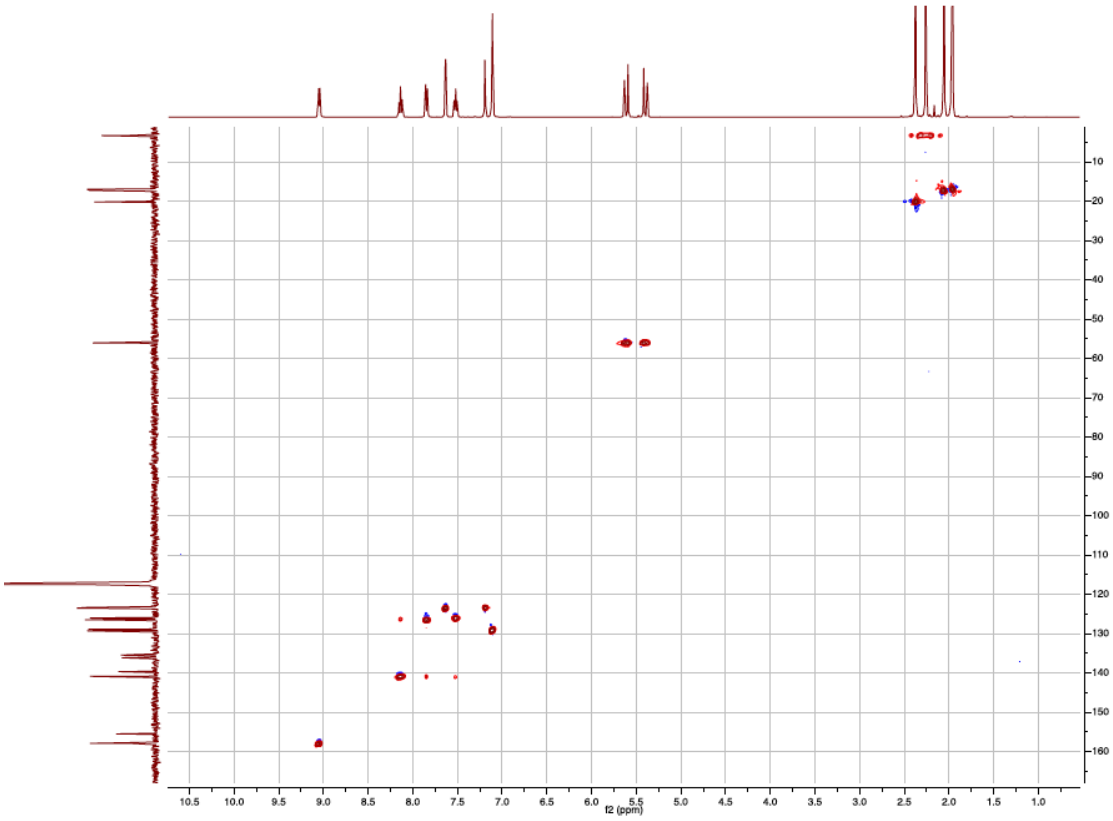

Figure S19. ^{1}H-^{13}C HSQC spectrum of **3·PF$_6$** dissolved in CD_3CN at 298K.

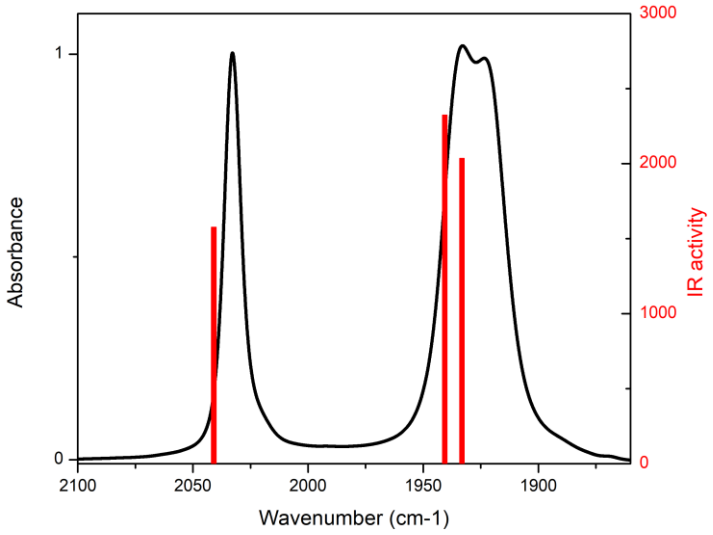

Figure S20. Lorentzian deconvolution of the IR spectra of **3·PF$_6$** in acetonitrile (black line). DFT calculated frequencies (red vertical bars).

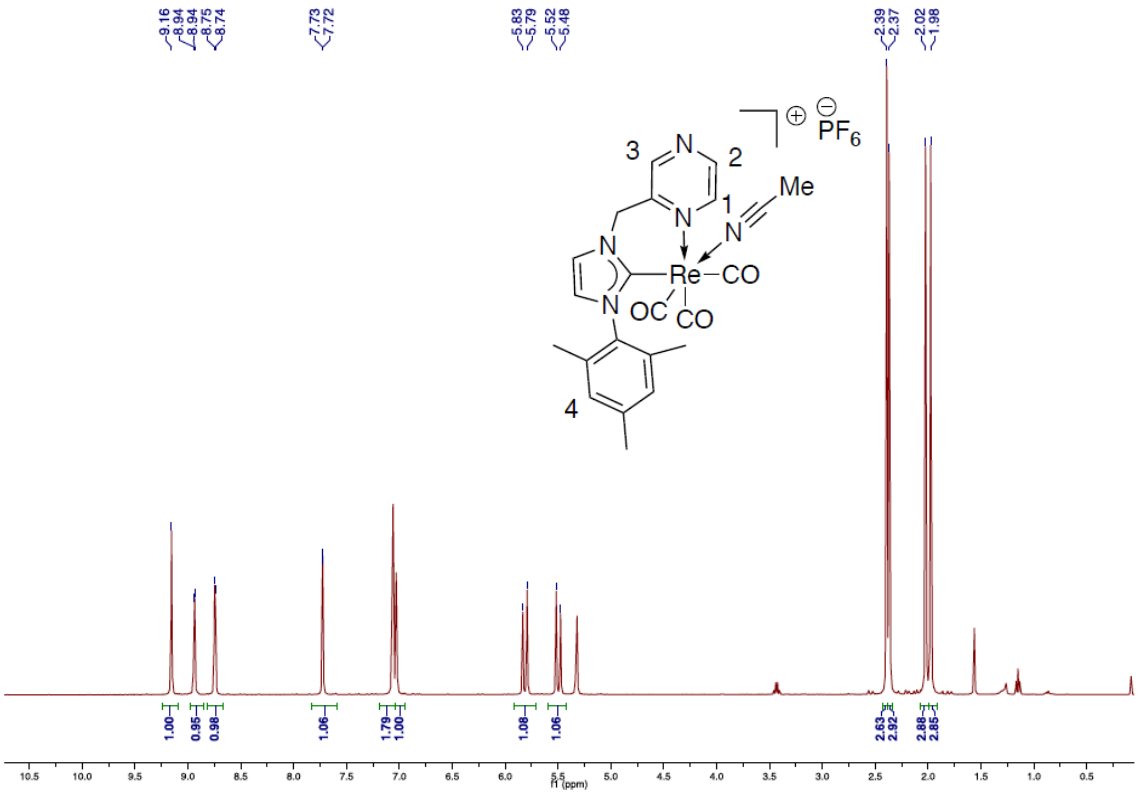

Figure S21. 400 MHz ^{1}H-NMR spectrum of **4·PF$_6$** dissolved in CD_2Cl_2 at 298K.

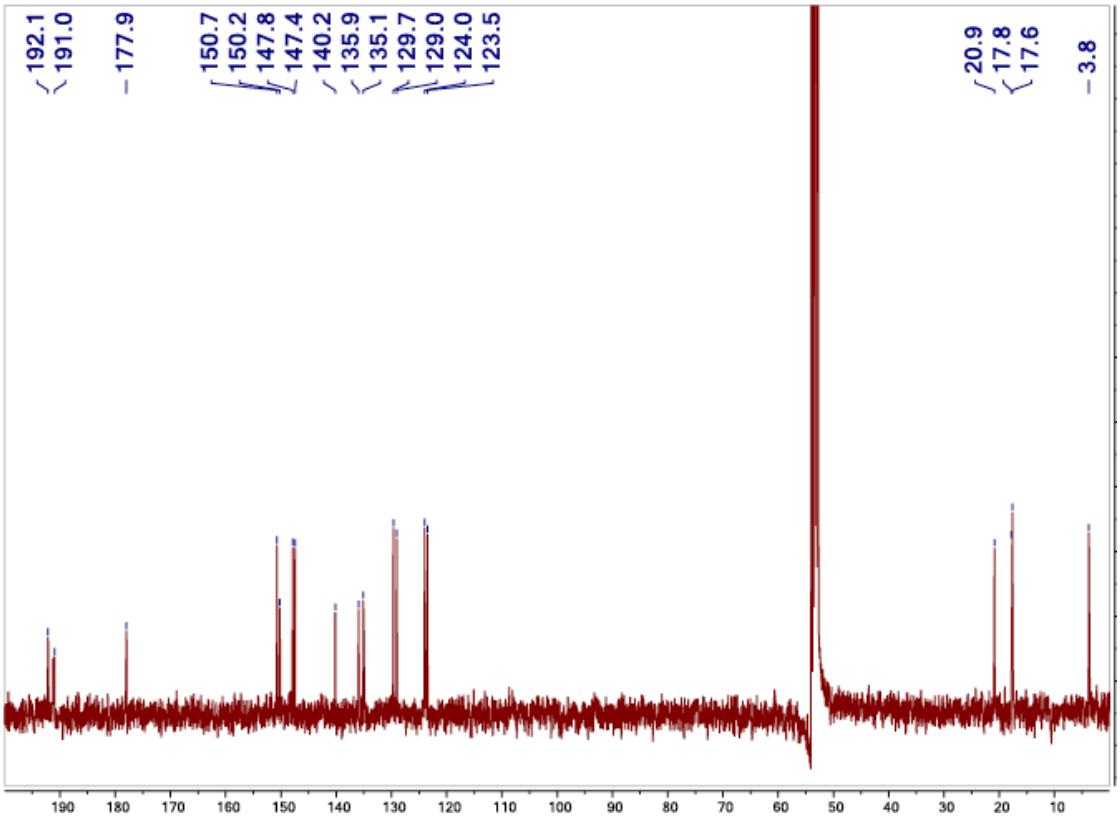

Figure S22. 100 MHz ^{1}H-NMR spectrum of **4·PF$_6$** dissolved in CD_2Cl_2 at 298K.

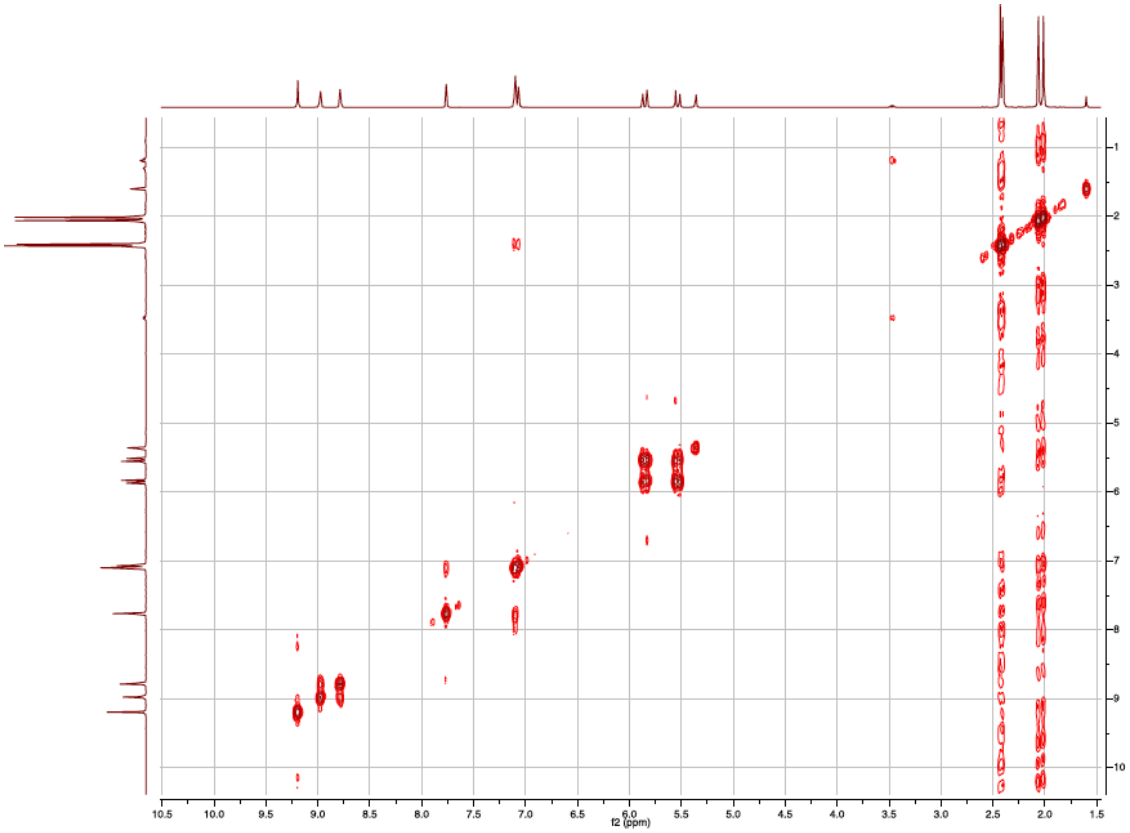

Figure S23. ^{1}H-^{1}H COSY spectrum of **4·PF$_6$** dissolved in CD_2Cl_2 at 298K.

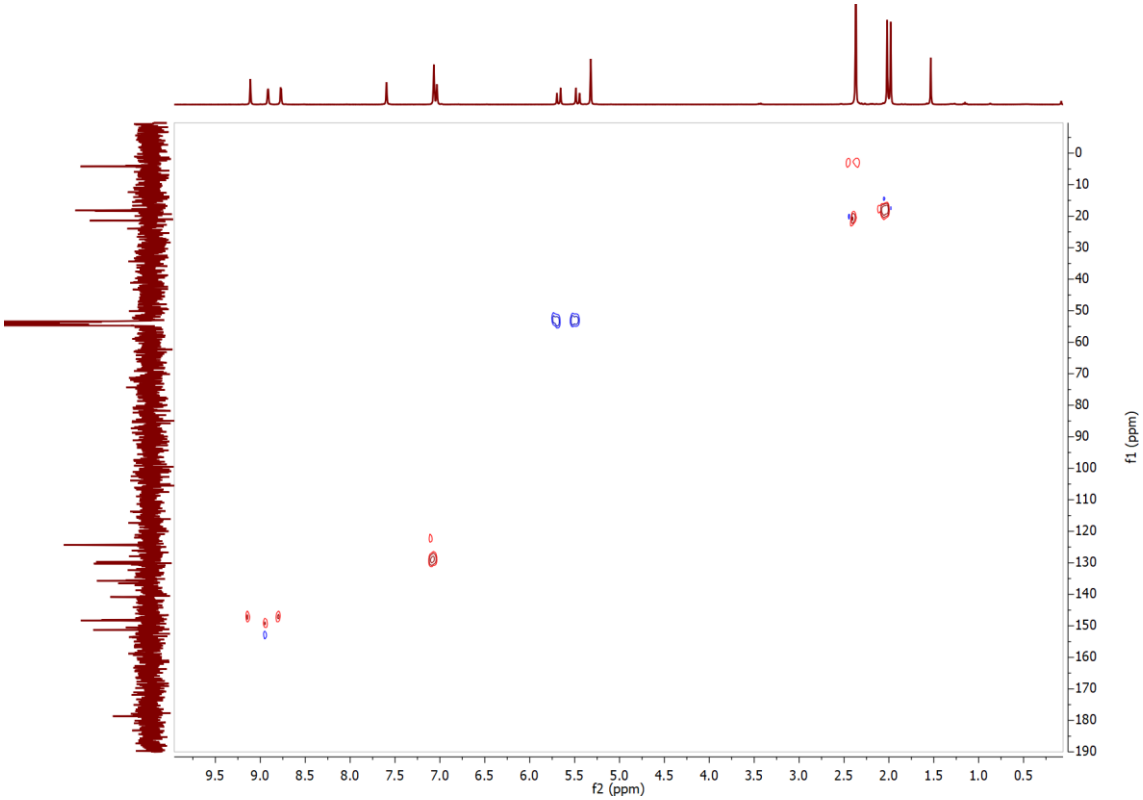

Figure S24. ^{1}H-^{13}C HSQC spectrum of **4·PF$_6$** dissolved in CD_2Cl_2 at 298K.

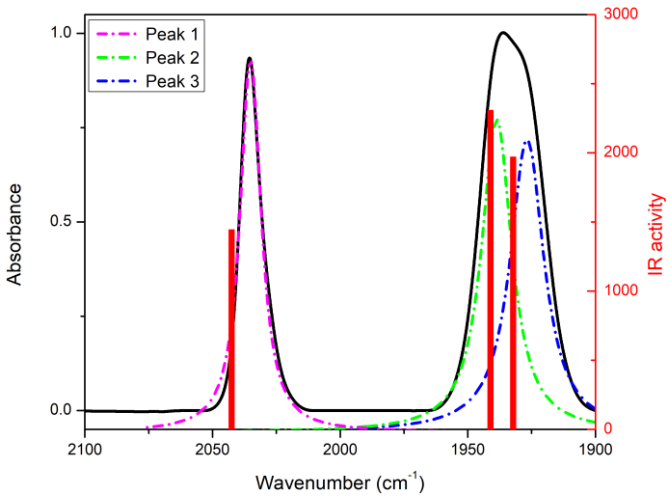

Peak	Area	Center (cm^{-1})	Width (cm^{-1})	Height
1	15.757	2035	9.345	1.073
2	17.806	1940	14.830	0.764
3	18.712	1926	17.096	0.697

DF	83
COD (R^2)	0.993
Reduced ChiSq	7.08E-4

Figure S25. Left: IR spectra of **4·PF$_6$** in acetonitrile (black line) with Lorentzian deconvolution (dash-dotted lines). DFT calculated frequencies (red vertical bars). Right: Fitted peak parameters obtained from Lorenztian deconvolution.

6. Electrochemistry.

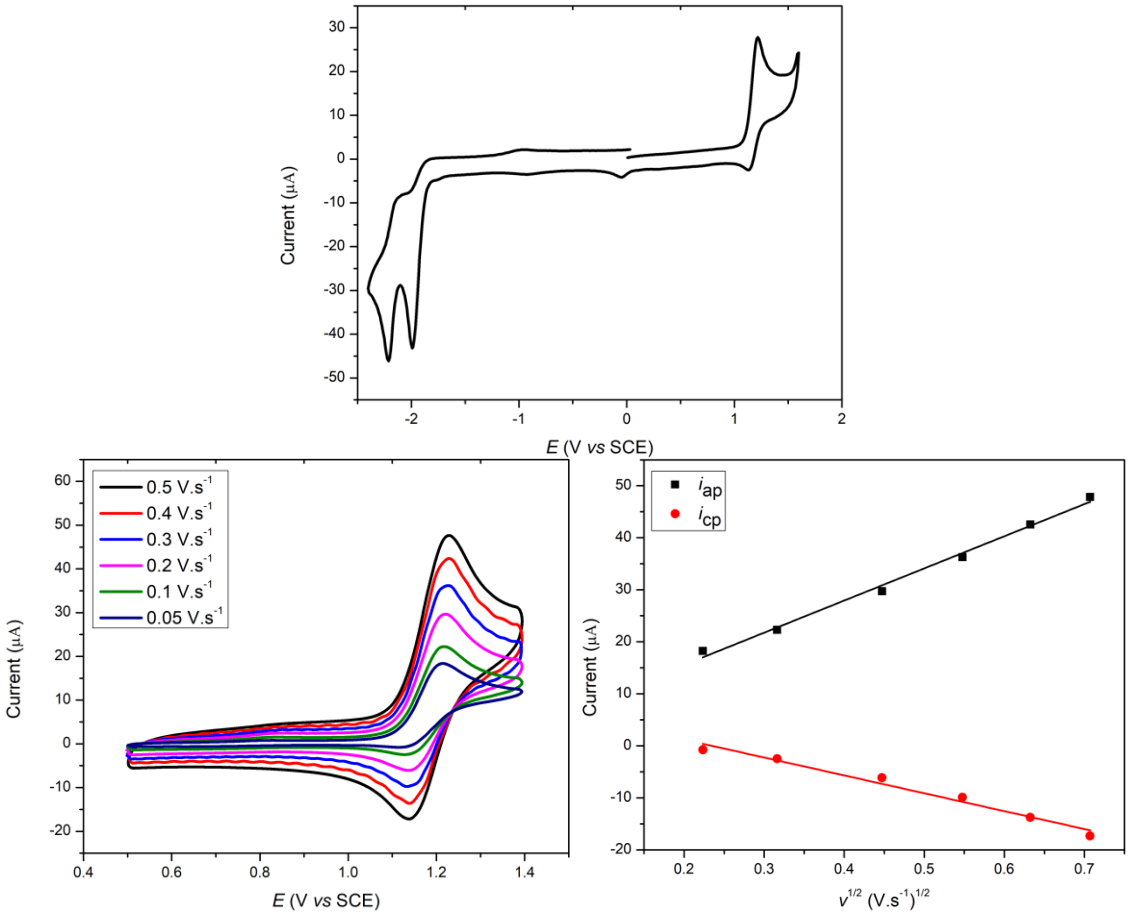

Figure S26. Top: Cyclic Voltammetry of **1**, in CH_3CN 0.1 M Bu_4NPF_6 at 298 K. v = 100 mV/s. Bottom left: Scan rate dependence of the $Re^{+2/+1}$ redox couple of **1**. Right: Plot of i_{ap}/i_{cp} *vs* $v^{1/2}$, where i_{ap} corresponds to the anodic peak and i_{cp} to the cathodic peak.

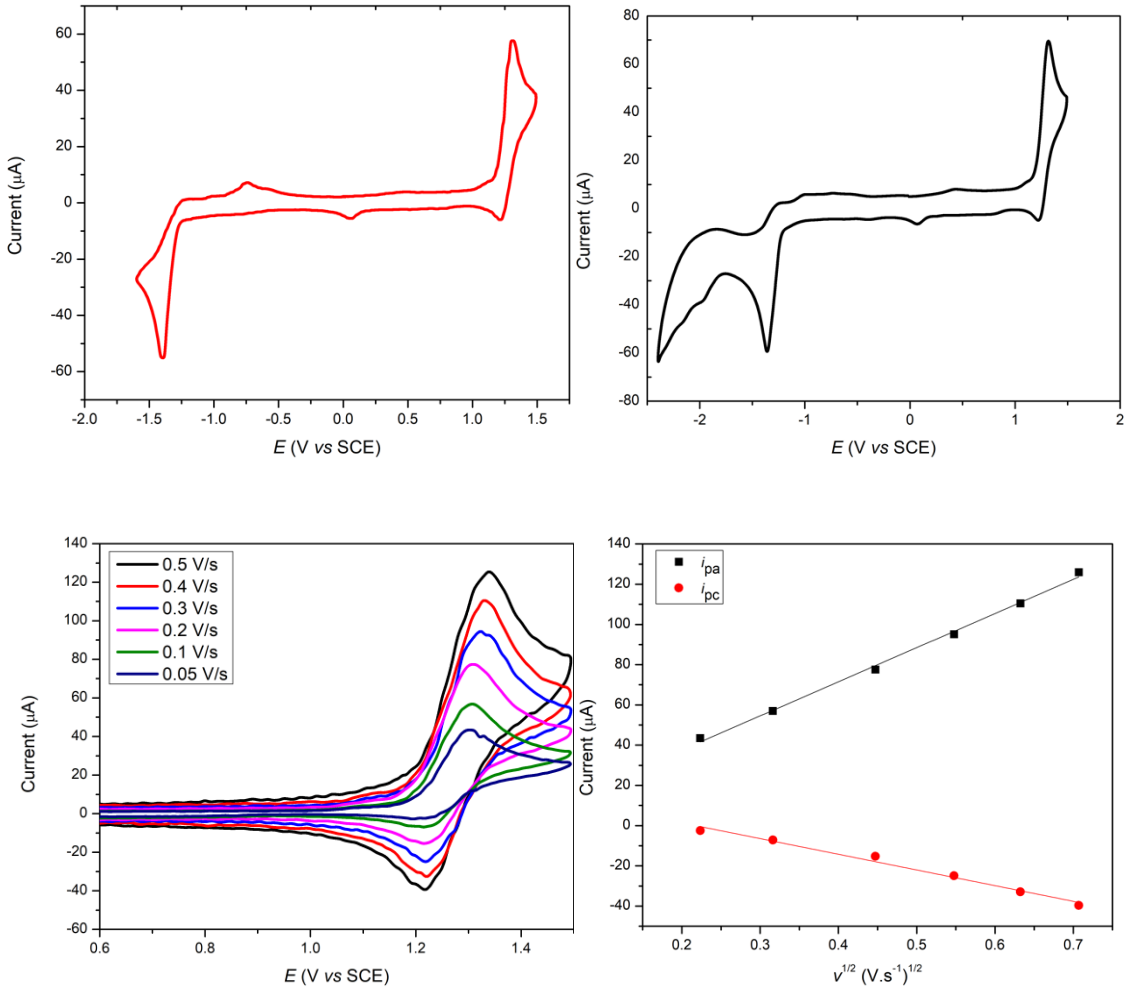

Figure S27. Top: Cyclic Voltammetry of **2**, in CH_3CN 0.1 M Bu_4NPF_6 at 298 K. v = 100 mV/s. Bottom left: Scan rate dependence of the $Re^{+2/+1}$ redox couple of **2**. Right: Plot of i_{ap}/i_{cp} *vs* $v^{1/2}$, where i_{ap} corresponds to the anodic peak and i_{cp} to the cathodic peak.

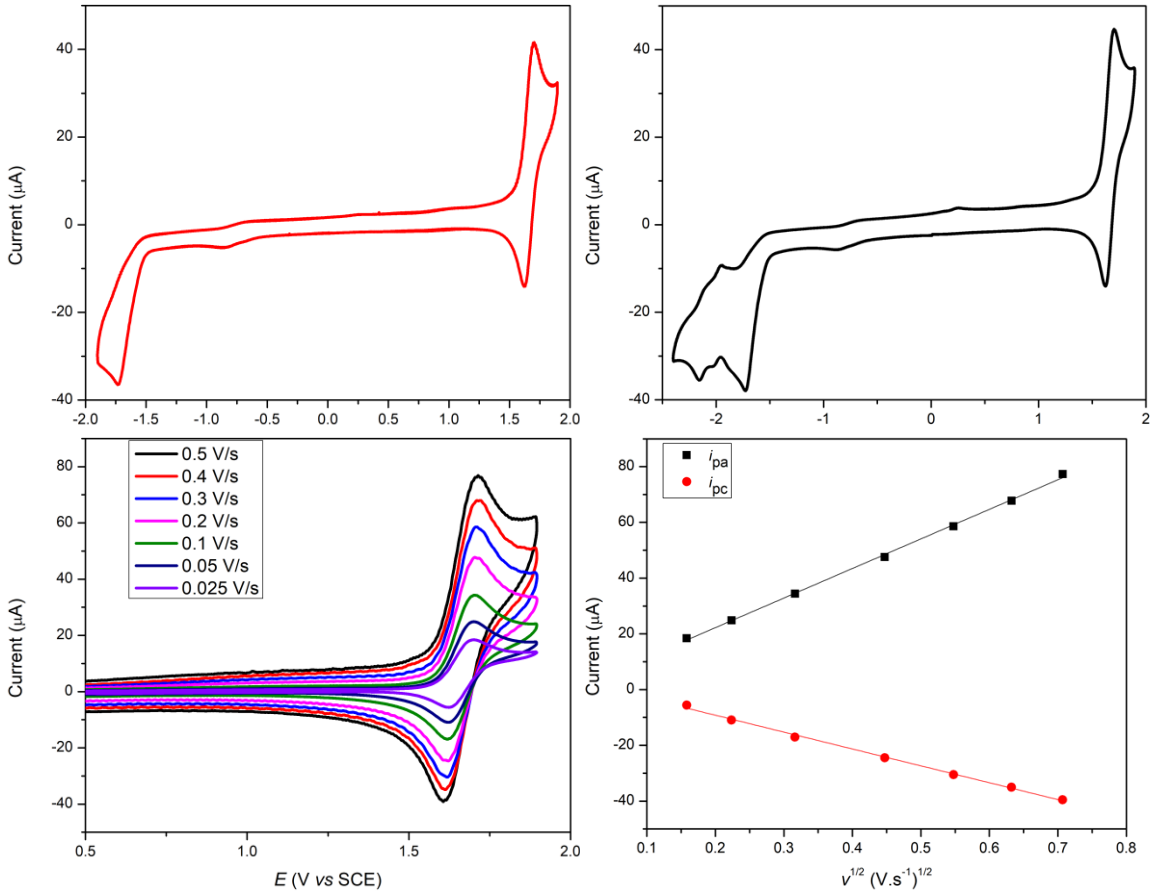

Figure S28. Top: Cyclic Voltammetry of **3·PF6**, in CH_3CN 0.1 M Bu_4NPF_6 at 298 K. v = 100 mV/s. Bottom left: Scan rate dependence of the $Re^{+2/+1}$ redox couple of **3·PF6**. Right: Plot of i_{ap}/i_{cp} *vs* $v^{1/2}$, where i_{ap} corresponds to the anodic peak and i_{cp} to the cathodic peak.

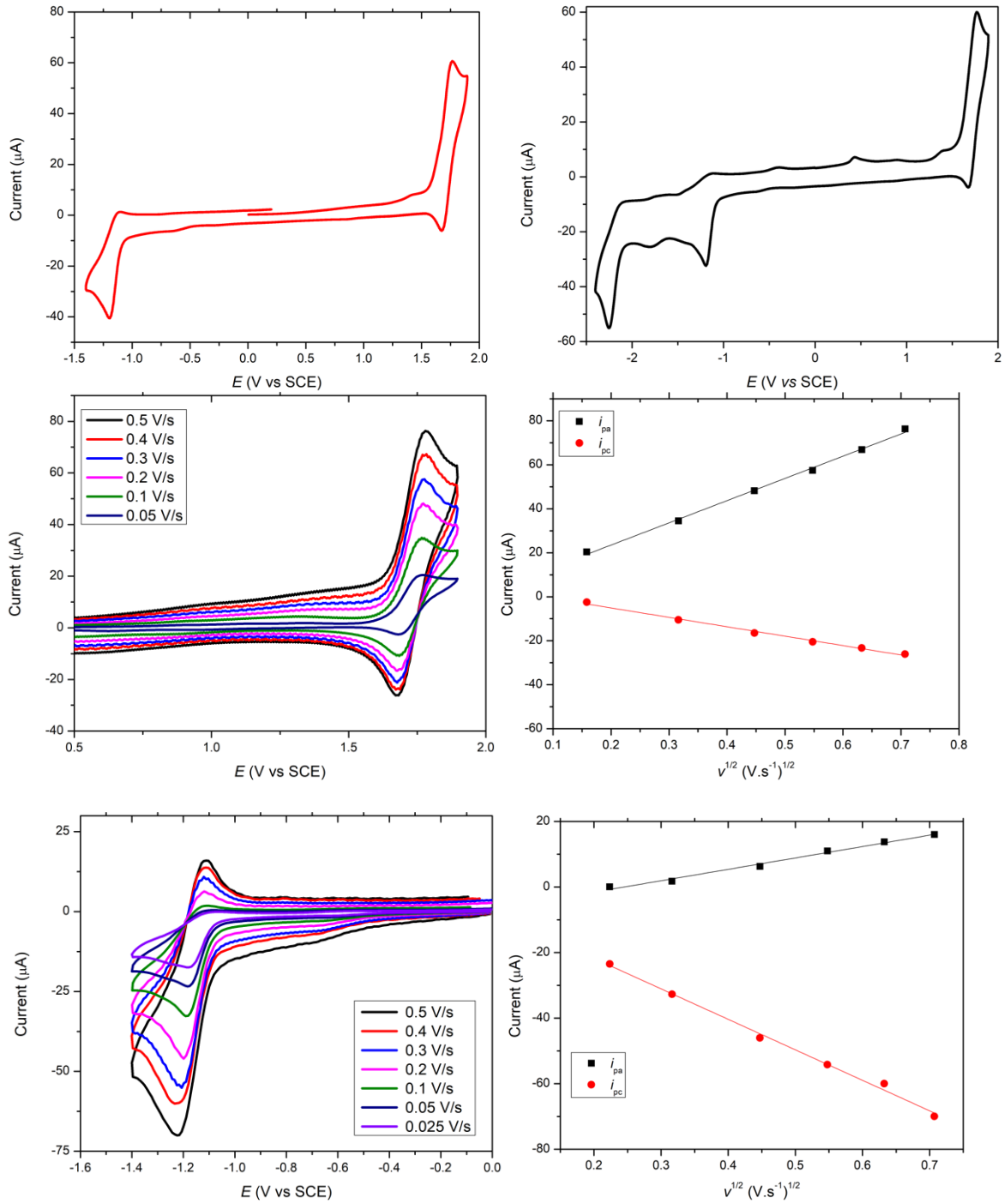

Figure S29. Top: Cyclic Voltammetry of **4·PF$_6$**, in CH_3CN 0.1 M Bu_4NPF_6 at 298 K. v = 100 mV/s. Center left: Scan rate dependence of the $Re^{+2/+1}$ redox couple of **4·PF$_6$**. Center right: Plot of i_{ap}/i_{cp} *vs* $v^{1/2}$, where i_{ap} corresponds to the anodic peak and i_{cp} to the cathodic peak. Bottom left: Scan rate dependence of the $pz^{0/-1}$ redox couple of **4·PF$_6$**. Bottom right: Plot of i_{ap}/i_{cp} *vs* $v^{1/2}$, where i_{ap} corresponds to the anodic peak and i_{cp} to the cathodic peak.

7. DFT calculations of the singlet and doublet ground state.

Table S1. DFT computed MO **1**, **2**, **3** and **4** in their singlet ground state in acetonitrile.

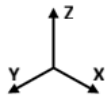	**1**	**2**	**3**	**4**
LUMO+3	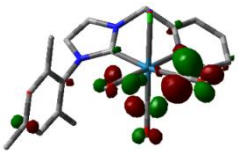 CO = 16%, NHC = 79 %,	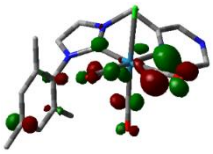 CO = 47%, NHC = 26%	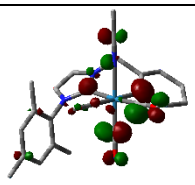 CO = 49%, NHC = 20%	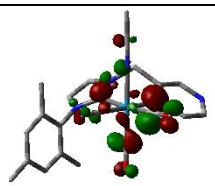 CO = 53%, NHC = 17 %
LUMO+2	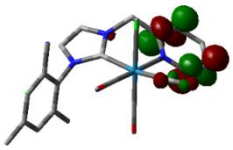 CO = 10%, py = 82%	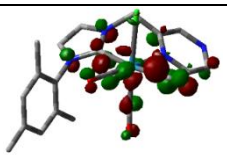 Re_{yz} = 22%, CO = 41%, NHC = 20 %, py = 15%	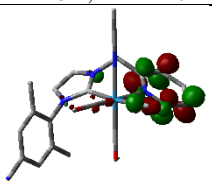 CO = 20%, py = 60%	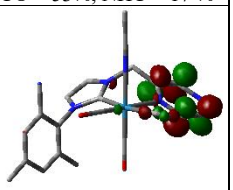 CO = 12%, pz = 75%
LUMO+1	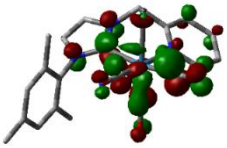 Re_{xz} = 18%, CO = 43%, NHC = 21 %, py = 16%	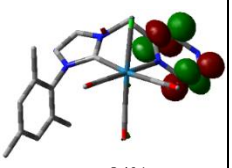 pz = 84%	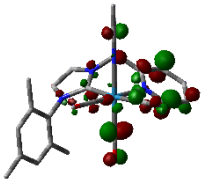 Re_{xz} = 17%, CO = 27%, py = 37%	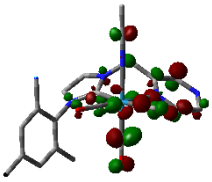 Re_{xz} = 25%, CO = 32%, pz = 24%
LUMO	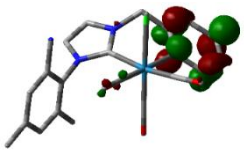 py = 85%	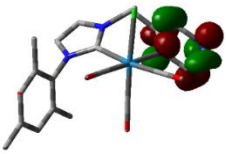 pz = 95%	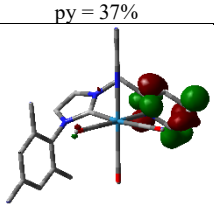 py = 89%	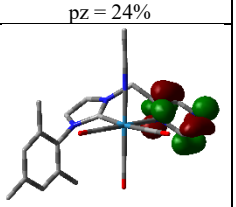 pz = 95%
HOMO	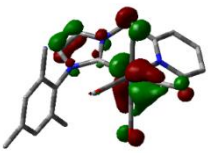 Re_{xz} = 39%, NHC = 23%, CO = 23 %, Cl = 12%	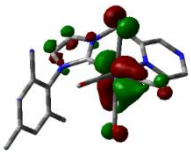 Re_{xz} = 45%, NHC = 17%, CO = 23 %, Cl = 14%	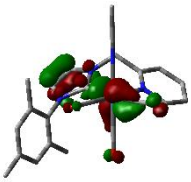 Re_{xz} = 44%, NHC = 19%, CO = 34%	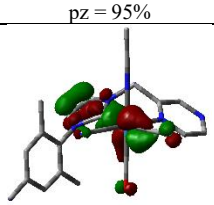 Re_{xz} = 42%, NHC = 36%, CO = 18%
HOMO-1	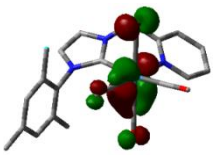 Re_{yz} = 48%, NHC = 3%, CO = 26 %, Cl = 19%	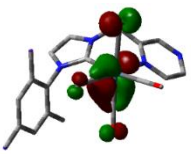 Re_{yz} = 50%, NHC = 3%, CO = 25 %, Cl = 19%	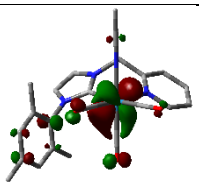 Re_{yz} = 52%, CO = 20%, NHC = 20%	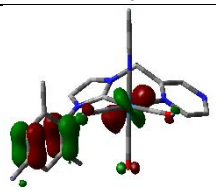 Re_{yz} = 33%, CO = 12%, NHC = 52%
HOMO-2	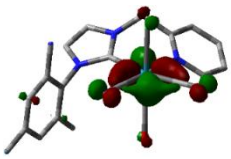 Re_{xy} = 39%, NHC = 23%, CO = 23 %, Cl = 12%	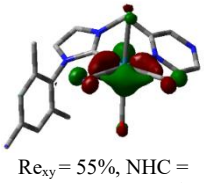 Re_{xy} = 55%, NHC = 12%, CO = 27 %, Cl = 5%	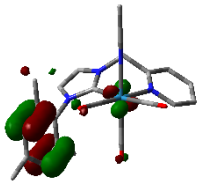 Re_{xy} = 14%, NHC = 78%	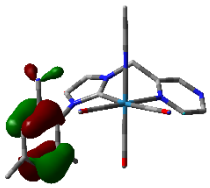 NHC = 96%

HOMO-3	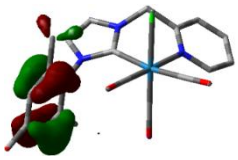 NHC = 98%	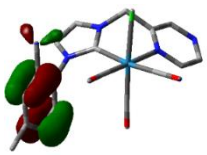 NHC = 99%	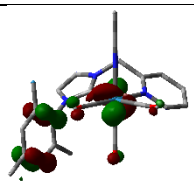 Re_{xy} = 37%, NHC = 45%	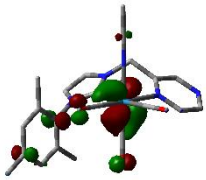 Re_{yz} = 50%, CO = 21%, NHC = 25%

Table S2. DFT computed spin densities of the one-electron oxidized and one-electron reduced species of **1**, **2**, **3** and **4** in their singlet ground state in acetonitrile.

compound	$-1e^-$	$+1e^-$
1	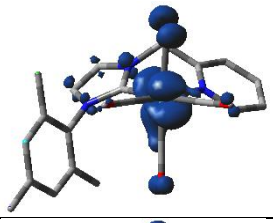	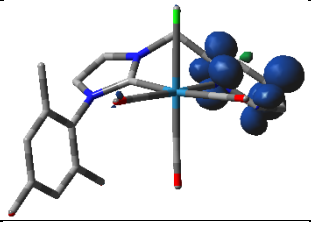
2	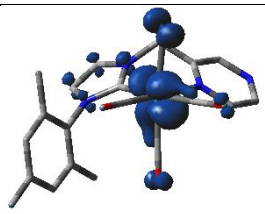	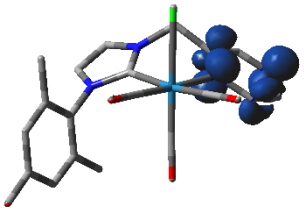
3	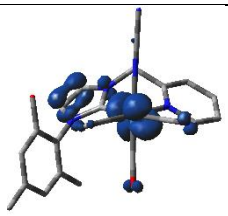	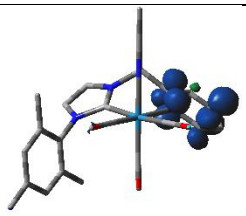
4	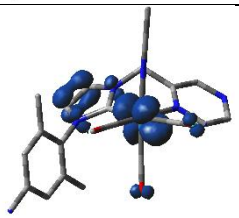	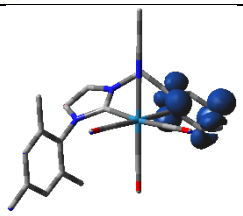

8. (TD)TDF of the singlet ground state.

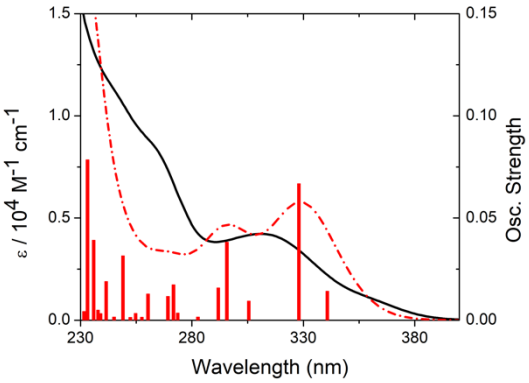

Figure S30. (TD)DFT-calculated (dashed curve) and experimental (solid curve) UV-Vis absorption spectra of complex **1** in their singlet ground state. Calculated transitions are represented by red vertical bars.

Table S3. (TD)DFT assignments for calculated UV-Vis transitions of complex **1** in their optimized singlet ground state.

No.	Wavelength (nm)	Osc. Strength	Major contribs
1	340	0.0142	HOMO->LUMO (94%)
2	327	0.0668	H-1->LUMO (89%)
4	295	0.0382	HOMO->L+1 (37%) HOMO->L+2 (45%)
5	291	0.0158	H-1->L+1 (27%) H-1->L+2 (50%)
8	271	0.0174	H-2->L+1 (21%) H-2->L+2 (26%)
14	249	0.0315	H-2->L+1 (45%) H-2->L+2 (28%)
19	235	0.0392	HOMO->L+4 (53%)
20	233	0.0785	H-6->LUMO (66%)

Table S4. Electron-density difference maps of transitions listed in **Table S3**. Violet and cyan show the regions of decreased and increased electron density respectively.

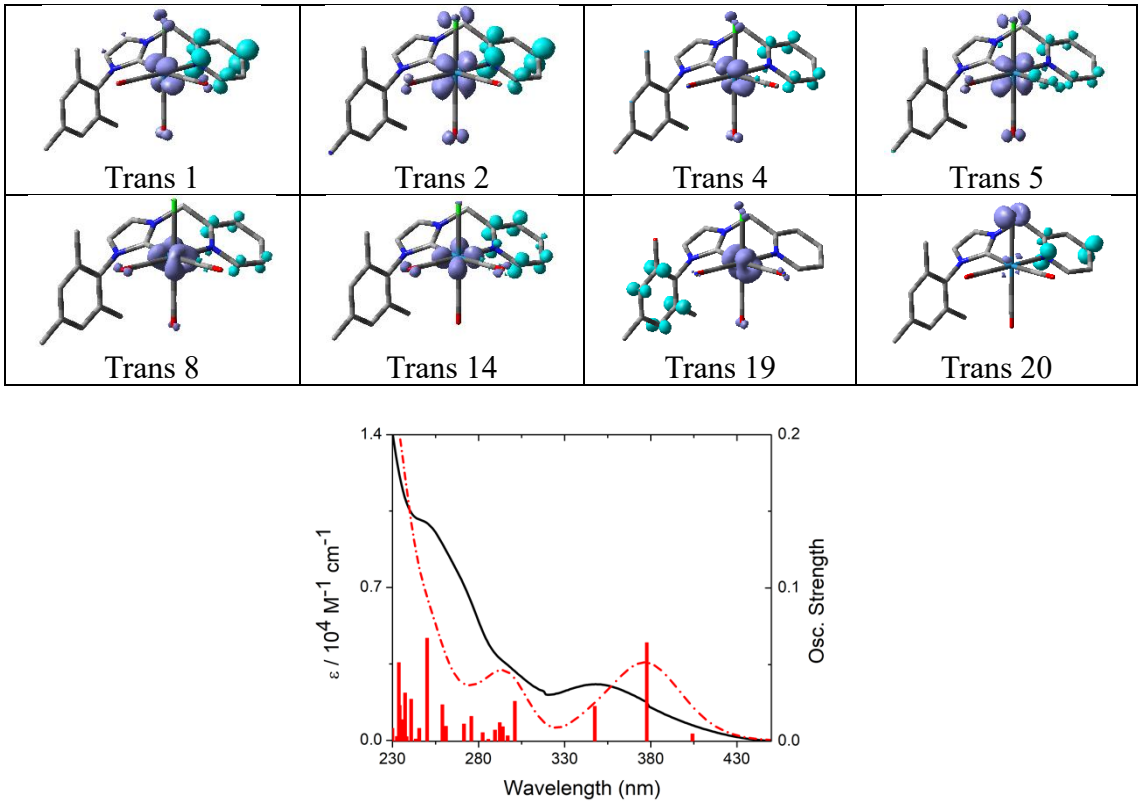

Figure S31. (TD)DFT-calculated (dashed curve) and experimental (solid curve) UV-Vis absorption spectra of complex **2** in their singlet ground state. Calculated transitions are represented by red vertical bars.

Table S5. (TD)DFT assignments for calculated UV-Vis transitions of complex **2** in their optimized singlet ground state.

No.	Wavelength (nm)	Osc. Strength	Major contribs
1	404	0.0048	HOMO->LUMO (97%)
2	377	0.0643	H-1->LUMO (94%)
3	347	0.0228	H-2->LUMO (90%)
4	301	0.0261	HOMO->L+1 (46%) HOMO->L+2 (37%)
8	292	0.0122	HOMO->L+1 (40%) HOMO->L+2 (38%)
12	275	0.0163	H-2->L+2 (54%)
13	271	0.0113	HOMO->L+3 (46%) HOMO->L+4 (16%)
15	258	0.0238	H-2->L+1 (65%)
16	250	0.0673	H-7->LUMO (45%) H-6->LUMO (33%)
19	240	0.0275	H-2->L+3 (31%) HOMO->L+5 (21%)

Table S6. Electron-density difference maps of transitions listed in **Table S5**. Violet and cyan show the regions of decreased and increased electron density respectively.

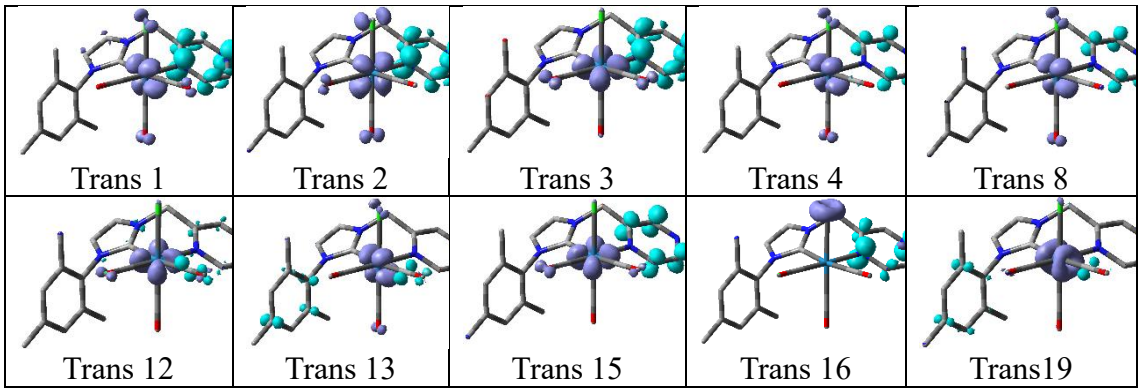

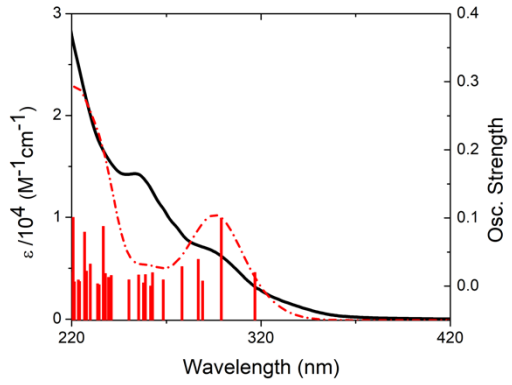

Figure S32. (TD)DFT-calculated (dashed curve) and experimental (solid curve) UV-Vis absorption spectra of complex **3**·PF_6 in their singlet ground state. Calculated transitions are represented by red vertical bars.

Table S7. (TD)DFT assignments for calculated UV-Vis transitions of complex **3** in their optimized singlet ground state.

No.	Wavelength (nm)	Osc. Strength	Major contribs
1	317	0.0202	HOMO->LUMO (95%)
2	299	0.1	H-1->LUMO (81%)
3	289	0.0076	H-4->LUMO (17%) H-3->LUMO (48%) H-2->LUMO (24%)
4	287	0.0395	HOMO->L+1 (64%) HOMO->L+2 (18%)
5	278	0.0287	H-1->L+1 (52%) H-1->L+2 (17%)
7	263	0.0199	H-3->L+1 (21%) HOMO->L+2 (25%)
9	259	0.0172	HOMO->L+2 (15%) HOMO->L+3 (41%)
10	258	0.005	H-4->LUMO (70%)
13	241	0.0159	H-1->L+4 (20%) HOMO->L+4 (17%)

Table S8. Electron-density difference maps of transitions listed in **Table S7**. Violet and cyan show the regions of decreased and increased electron density respectively.

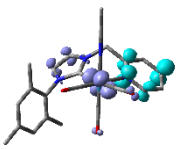 Trans 1	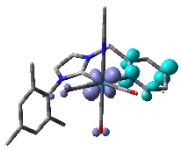 Trans 2	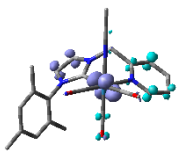 Trans 3
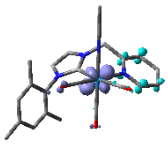 Trans 4	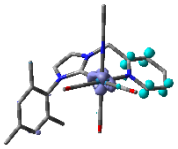 Trans 5	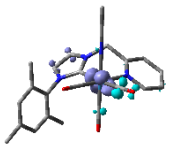 Trans 7
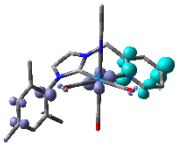 Trans 9	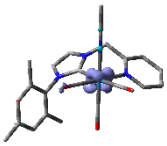 Trans 10	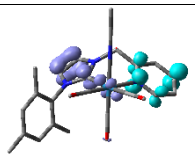 Trans 13

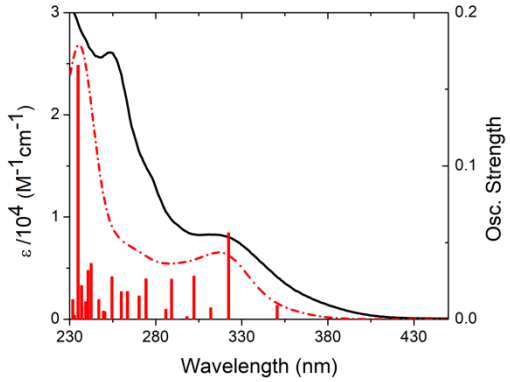

Figure S33. (TD)DFT-calculated (dashed curve) and experimental (solid curve) UV-Vis absorption spectra of complex **4·PF$_6$** in their singlet ground state. Calculated transitions are represented by red vertical bars.

Table S9. (TD)DFT assignments for calculated UV-Vis transitions of complex **4** in their optimized singlet ground state.

No.	Wavelength (nm)	Osc. Strength	Major contribs
1	350	0.0091	HOMO->LUMO (97%)
2	322	0.0564	H-1->LUMO (77%)
4	302	0.0283	HOMO->L+1 (69%) HOMO->L+2 (12%)
7	289	0.0262	H-4->L+1 (13%) H-1->L+1 (40%)
9	274	0.0264	H-4->L+1 (25%) H-3->L+1 (34%)
11	264	0.0182	H-5->LUMO (61%) HOMO->L+3 (21%)
13	255	0.0278	H-3->L+3 (15%) H-1->L+2 (36%)
17	242	0.0365	H-4->L+2 (19%) H-3->L+2 (30%)
18	241	0.0319	H-6->L+2 (20%) H-4->L+3 (18%) H-3->L+3 (16%)
22	235	0.1658	H-7->LUMO (23%) HOMO->L+4 (26%)

Table S10. Electron-density difference maps of transitions listed in **Table S9**. Violet and cyan show the regions of decreased and increased electron density respectively.

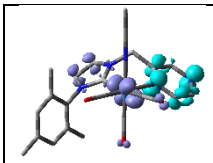 Trans 1	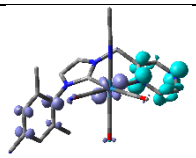 Trans 2	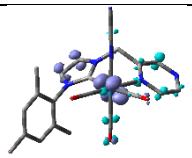 Trans 4	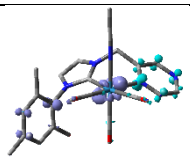 Trans 7	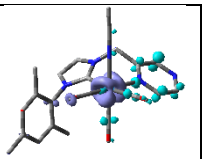 Trans 9
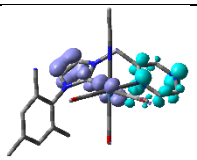 Trans 11	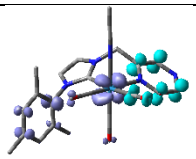 Trans 13	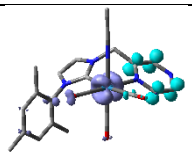 Trans 17	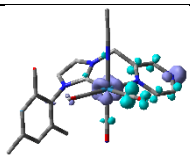 Trans 18	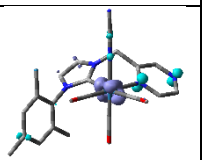 Trans 22

9. UV-Vis Spectroelectrochemistry.

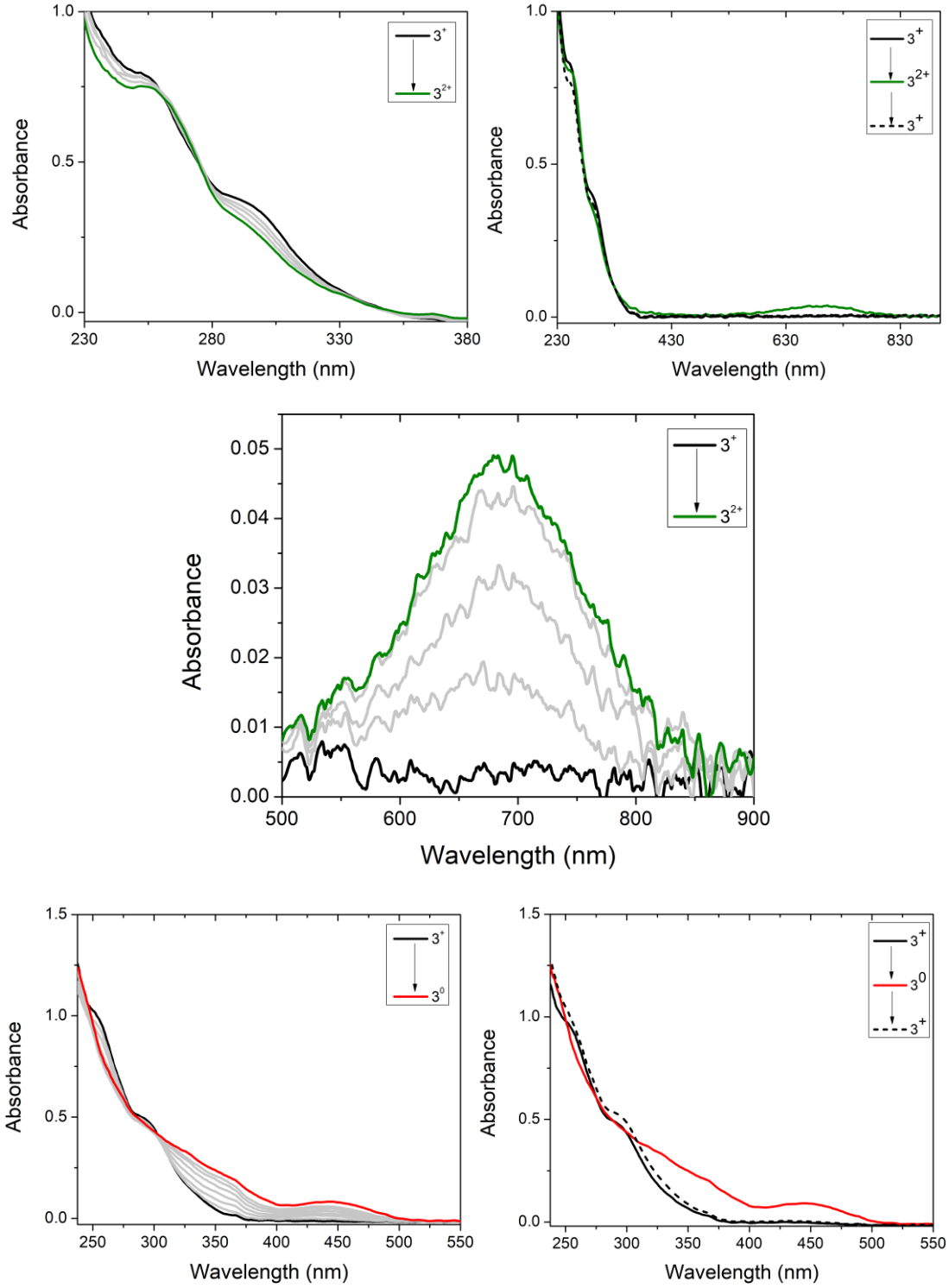

Figure S34. UV-Vis spectroelectrochemistry of complexes **3·PF$_6$** acetonitrile (0.1M Bu_4NPF_6). Conditions: WE (platinum), CE (platinum) and RE (Ag/AgCl 3M KCl). Changes recorded after one-electron oxidation and one-electron reduction process of complexes **3·PF$_6$**.

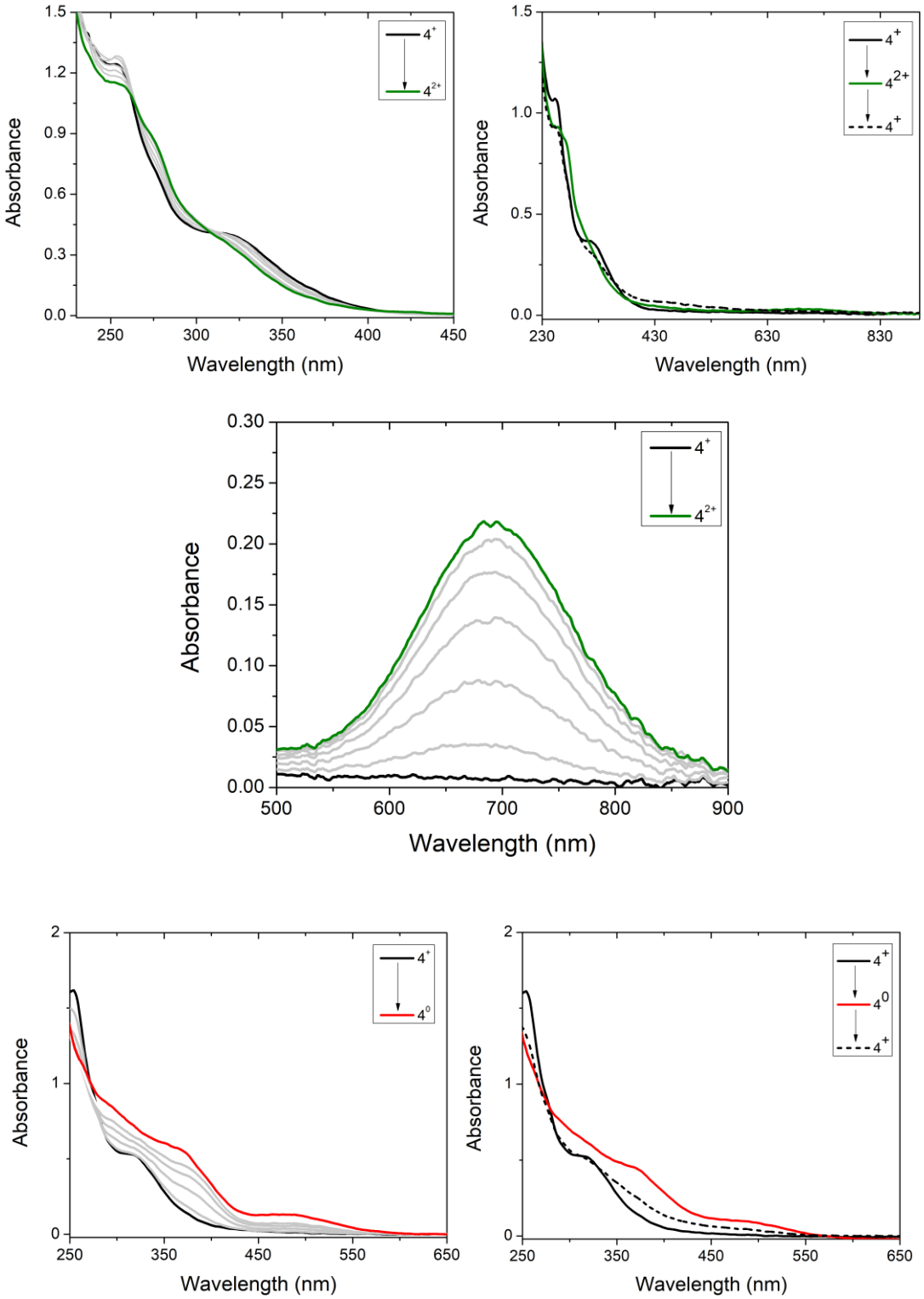

Figure S35. UV-Vis spectroelectrochemistry of complexes **4·PF$_6$** acetonitrile (0.1M Bu_4NPF_6). Conditions: WE (platinum), CE (platinum) and RE (Ag/AgCl 3M KCl). Changes recorded after one-electron oxidation and one-electron reduction process of complexes **4·PF$_6$**.

10. (TD)TDF of the one-electron oxidized and one-electron reduced species of 3 and 4 in their singlet ground state.

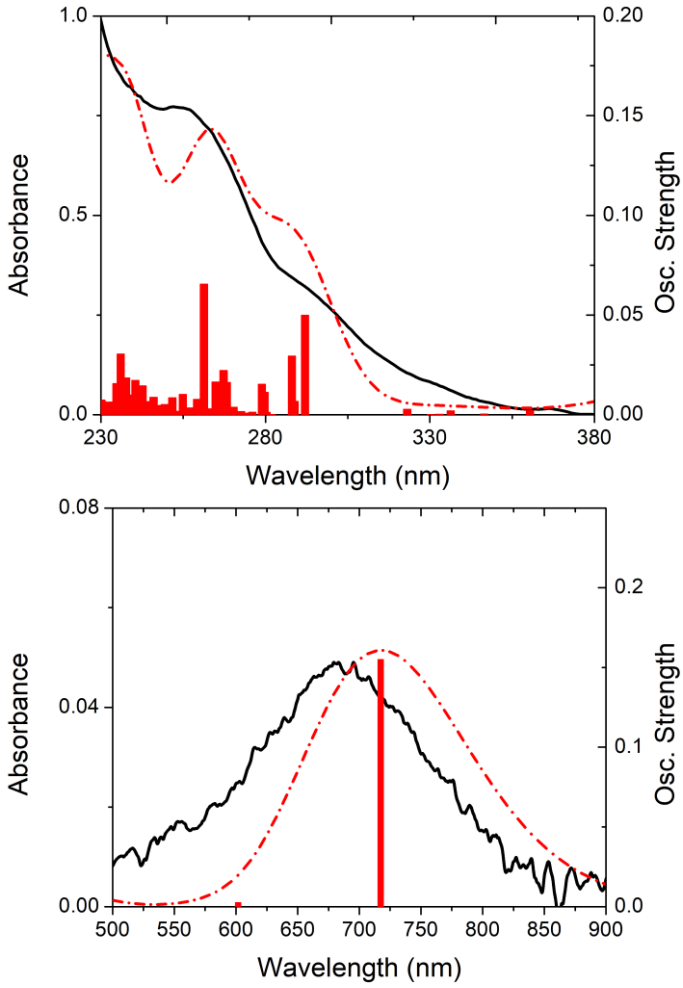

Figure S36. (TD)DFT-calculated (dashed curve) and experimental (solid curve) UV-Vis absorption spectra of complex **3·PF$_6$** in their one-electron oxidized doublet ground state. Calculated transitions are represented by red vertical bars.

Table S11. (TD)DFT assignments for calculated UV-Vis transitions of complex **3**$^+$ in their optimized doublet ground state.

No.	Wavelength (nm)	Osc. Strength	Major contribs
5	717	0.155	H-4(β)->LUMO(β) (91%)
17	292	0.05	H-2(α)->LUMO(A) (30%) H-2(α)->L+1(α) (17%) H-2(β)->L+2(β) (17%)
19	288	0.0295	H-2(α)->LUMO(α) (17%) H-12(β)->LUMO(β) (26%)
34	261	0.0656	H-3(α)->LUMO(α) (19%) H-1(α)->L+1(α) (21%) H-2(β)->L+1(β) (20%)

Table S12. Electron-density difference maps of transitions listed in **Table S11**. Violet and cyan show the regions of decreased and increased electron density respectively.

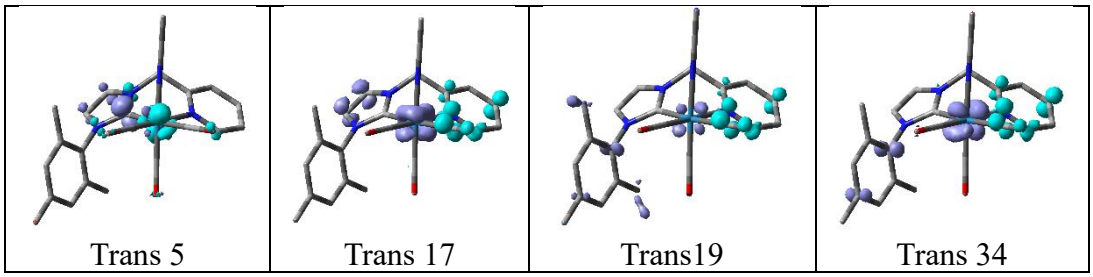

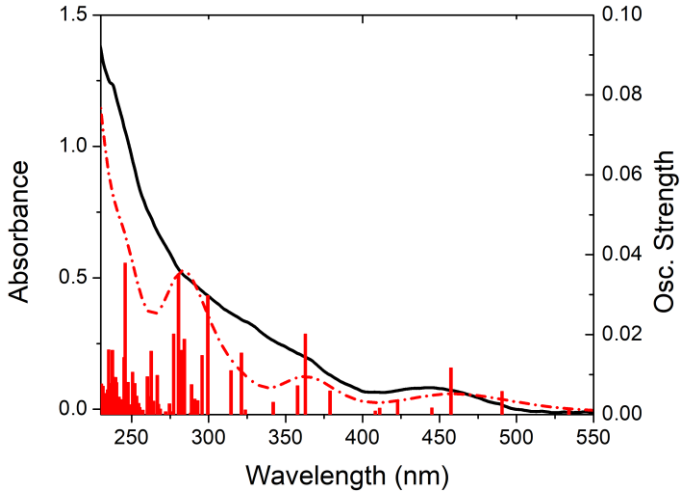

Figure S37. (TD)DFT-calculated (dashed curve) and experimental (solid curve) UV-Vis absorption spectra of complex **3**·$\mathbf{PF_6}$ in their one-electron reduced doublet ground state. Calculated transitions are represented by red vertical bars.

Table S13. (TD)DFT assignments for calculated UV-Vis transitions of complex $\mathbf{3^0}$ in their optimized doublet ground state.

No.	Wavelength (nm)	Osc. Strength	Major contribs
8	491	0.0058	HOMO(α)->L+6(α) (12%) HOMO(α)->L+7(α) (83%)
9	457	0.0117	HOMO(α)->L+8(α) (71%) HOMO(α)->L+9(α) (14%) HOMO(α)->L+10(α) (11%)
15	363	0.0202	HOMO(α)->L+15(α) (93%)
20	321	0.0154	H-1(α)->LUMO(α) (27%) H-1(B)->LUMO(B) (17%) HOMO(B)->LUMO(B) (33%)
22	299	0.0298	H-2(α)->LUMO(α) (20%) HOMO(β)->LUMO(β) (13%) HOMO(β)->L+1(β) (14%)
30	280	0.0352	H-1(α)->LUMO(α) (15%) H-1(α)->L+1(α) (11%) H-1(β)->LUMO(β) (19%) H-1(β)->L+1(β) (11%)

Table S14. Electron-density difference maps of transitions listed in **Table S13**. Violet and cyan show the regions of decreased and increased electron density respectively.

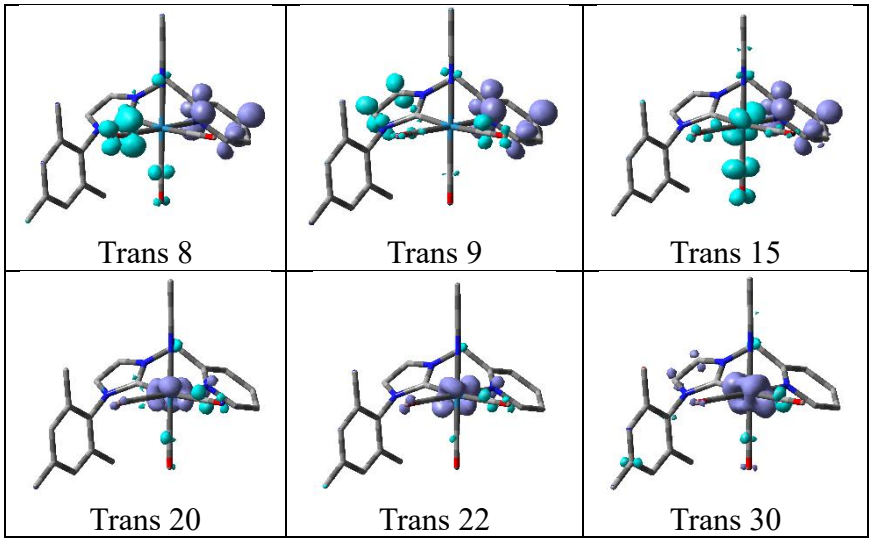

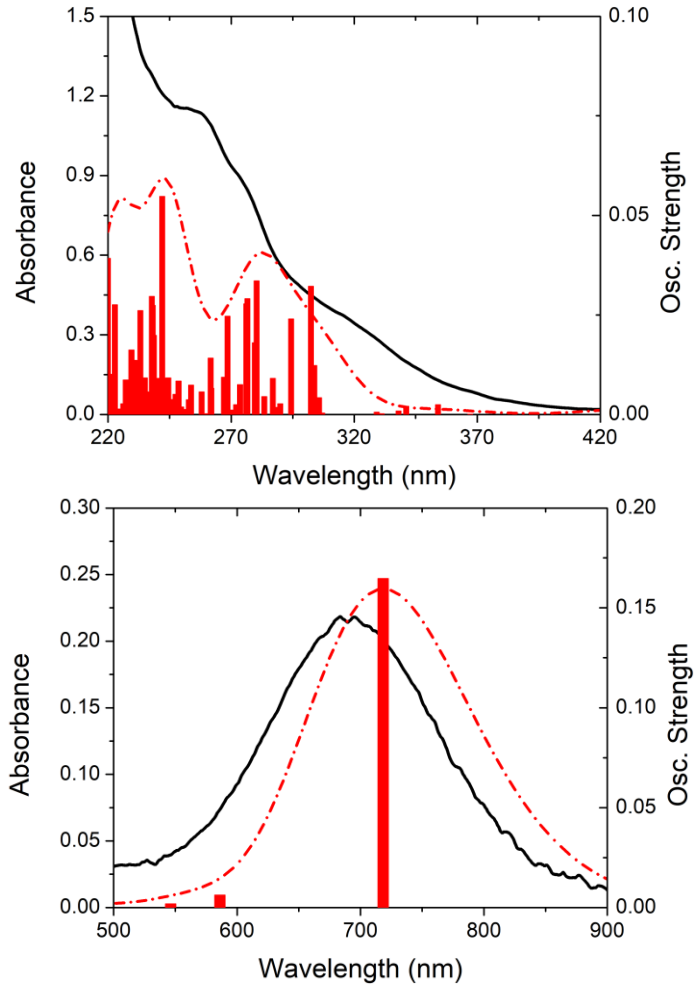

Figure S38. (TD)DFT-calculated (dashed curve) and experimental (solid curve) UV-Vis absorption spectra of complex **4**·$\mathbf{PF_6}$ in their one-electron oxidized doublet ground state. Calculated transitions are represented by red vertical bars.

Table S15. (TD)DFT assignments for calculated UV-Vis transitions of complex $\mathbf{4}^{+}$ in their optimized doublet ground state.

No.	Wavelength (nm)	Osc. Strength	Major contribs
5	718	0.1648	H-4(β)->LUMO(β) (91%)
20	307	0.0322	H-1(α)->LUMO(α) (39%) H-1(β)->L+1(β) (48%)
22	299	0.024	H-5(α)->LUMO(α) (37%) H-2(α)->LUMO(α) (24%) H-5(β)->L+1(β) (25%)
27	285	0.0336	H-2(α)->L+1(α) (41%) H-3(β)->L+1(β) (27%)
29	282	0.0291	H-3(α)->LUMO(α) (32%) HOMO(α)->L+1(α) (14%)
34	274	0.0247	H-1(α)->L+1(α) (21%) H-3(β)->L+2(β) (21%) H-1(β)->L+2(β) (18%)
51	247	0.0548	H-6(β)->L+1(β) (11%) H-2(β)->L+3(β) (22%) H-1(β)->L+3(β) (23%)

Table S16. Electron-density difference maps of transitions listed in **Table S15**. Violet and cyan show the regions of decreased and increased electron density respectively.

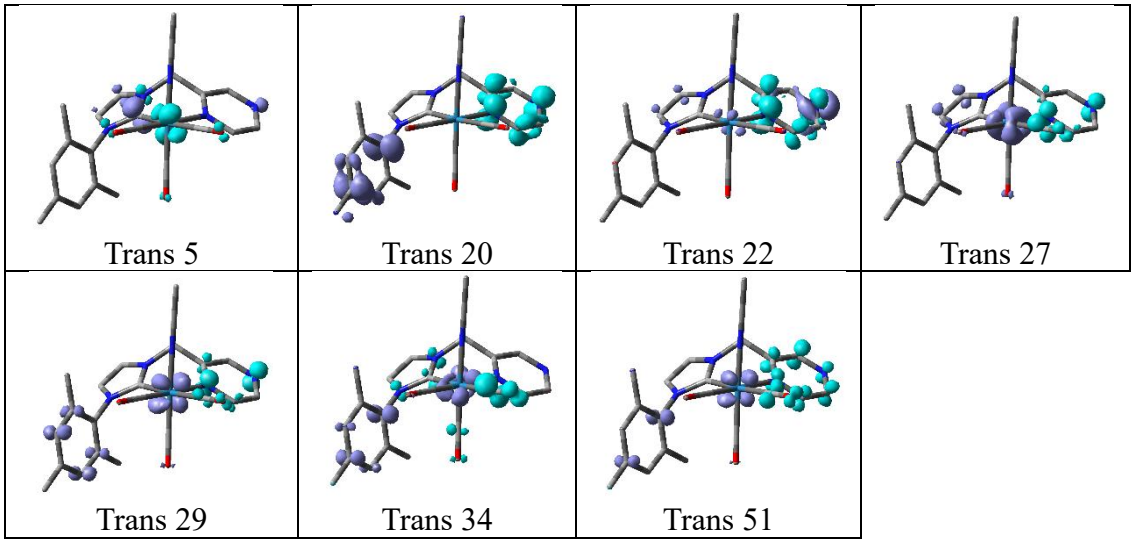

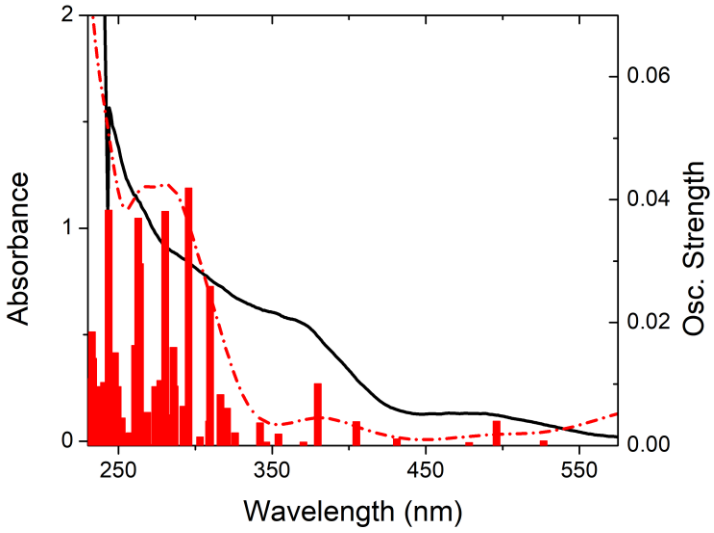

Figure S39. (TD)DFT-calculated (dashed curve) and experimental (solid curve) UV-Vis absorption spectra of complex **4·PF$_6$** in their one-electron reduced doublet ground state. Calculated transitions are represented by red vertical bars.

Table S17. (TD)DFT assignments for calculated UV-Vis transitions of complex **4^0** in their optimized doublet ground state.

No.	Wavelength (nm)	Osc. Strength	Major contribs
5	496	0.004	HOMO(α)->L+2(α) (64%) HOMO(α)->L+4(α) (24%)
8	405	0.0039	HOMO(α)->L+7(α) (85%)
9	380	0.0101	HOMO(α)->L+8(α) (59%) HOMO(α)->L+9(α) (31%)
18	310	0.0259	H-2(α)->LUMO(α) (14%) H-1(β)->LUMO(β) (33%) HOMO(β)->LUMO(β) (14%)
21	296	0.0419	H-4(β)->L+6(β) (10%)
27	280	0.0381	H-1(α)->LUMO(α) (21%) HOMO(β)->L+1(β) (19%)
37	263	0.037	H-4(β)->LUMO(β) (37%)

Table S18. Electron-density difference maps of transitions listed in **Table S17**. Violet and cyan show the regions of decreased and increased electron density respectively.

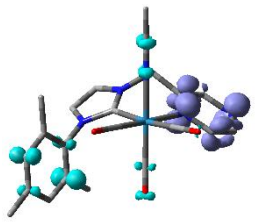 Trans 5	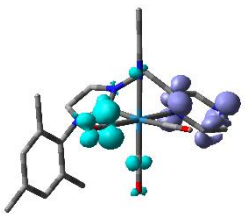 Trans 8	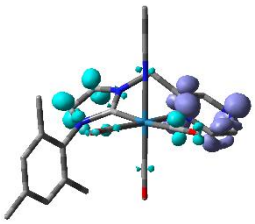 Trans 9	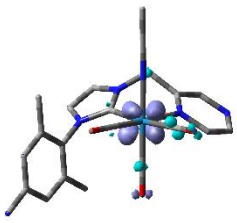 Trans 18
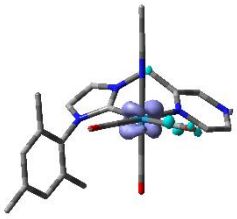 Trans 21	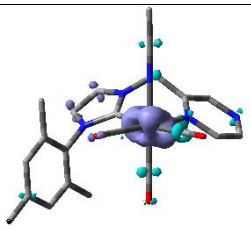 Trans 27	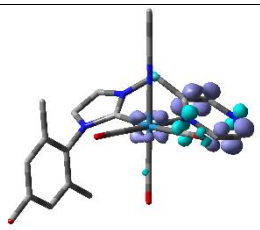 Trans 37	

11. Acid effects: Electrochemistry and 1H NMR spectra.

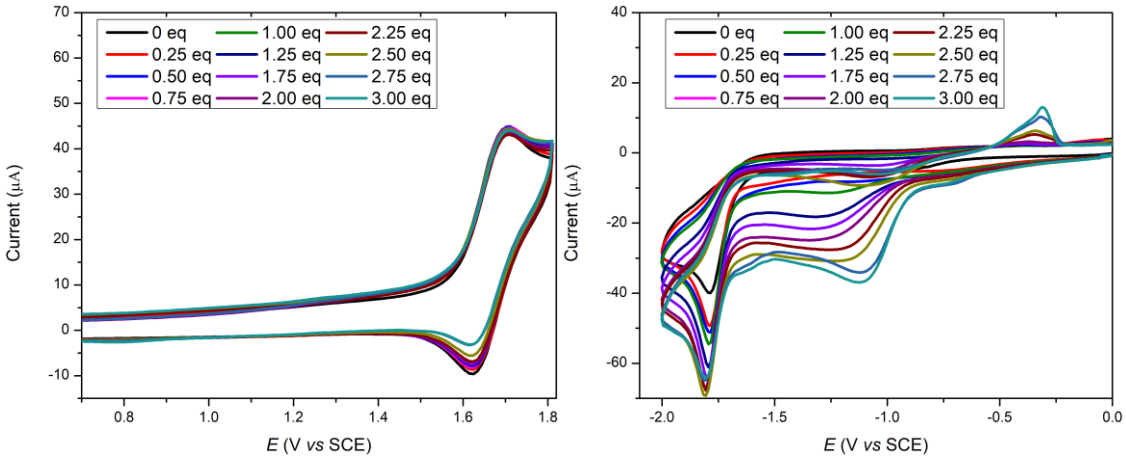

Figure S40. Oxidative (left) and reductive (right) Cyclic Voltammetry of **3·PF$_6$** upon addition of $B(C_6F_5)_3$ in 0.1 M Bu_4NPF_6 at 298 K. v = 100 mV/s.

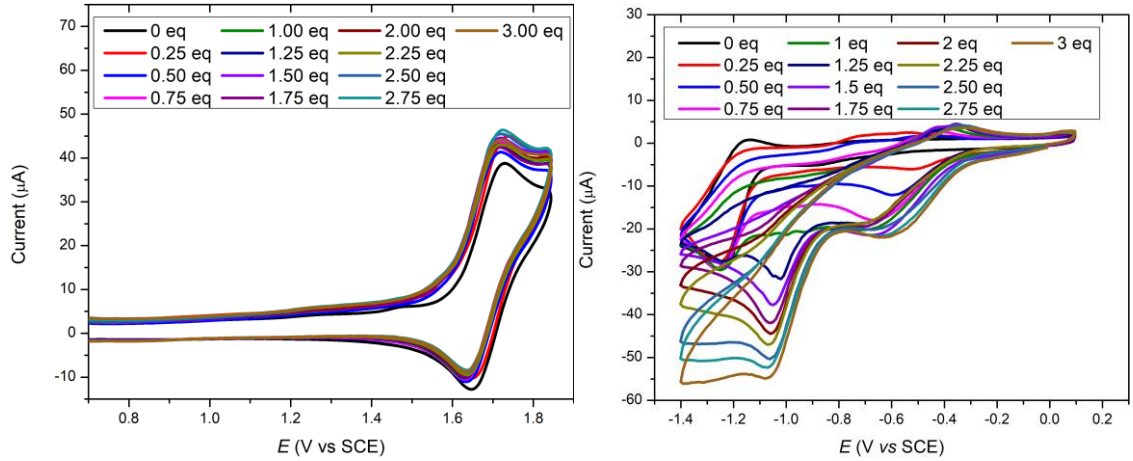

Figure S41. Oxidative (left) and reductive (right) Cyclic Voltammetry of **4·PF$_6$** upon addition of $B(C_6F_5)_3$ in 0.1 M Bu_4NPF_6 at 298 K. v = 100 mV/s.

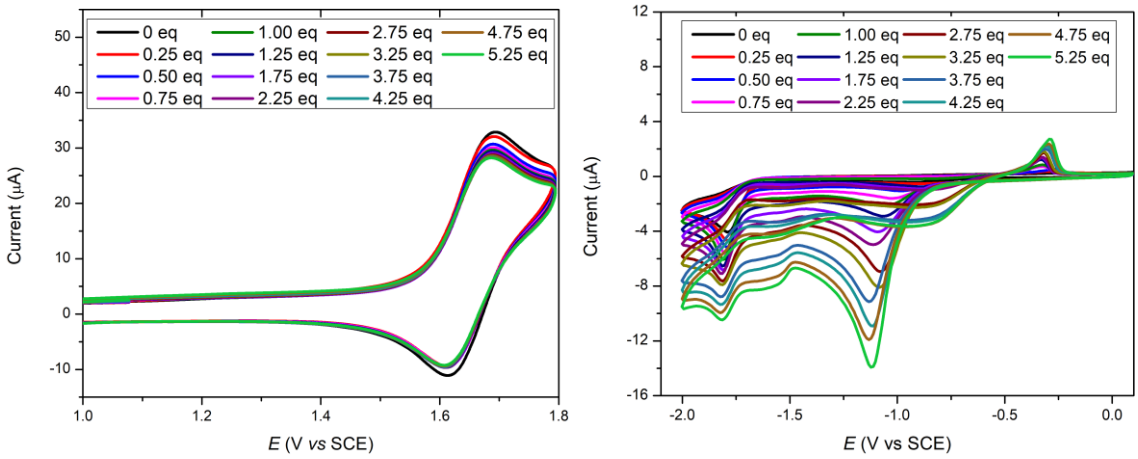

Figure S42. Oxidative Cyclic Voltammetry of **3·PF$_6$** upon addition of TfOH in 0.1 M Bu_4NPF_6 at 298 K. v = 100 mV/s.

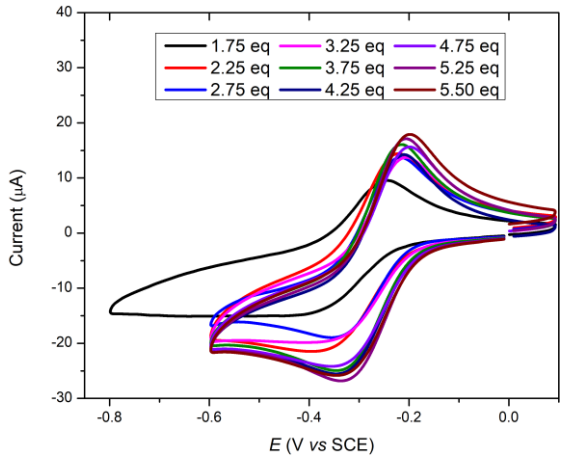

Figure S43. Reductive Cyclic Voltammetry of **4·PF$_6$** upon addition of TfOH in CH_3CN 0.1 M Bu_4NPF_6 at 298 K. v = 100 mV/s.

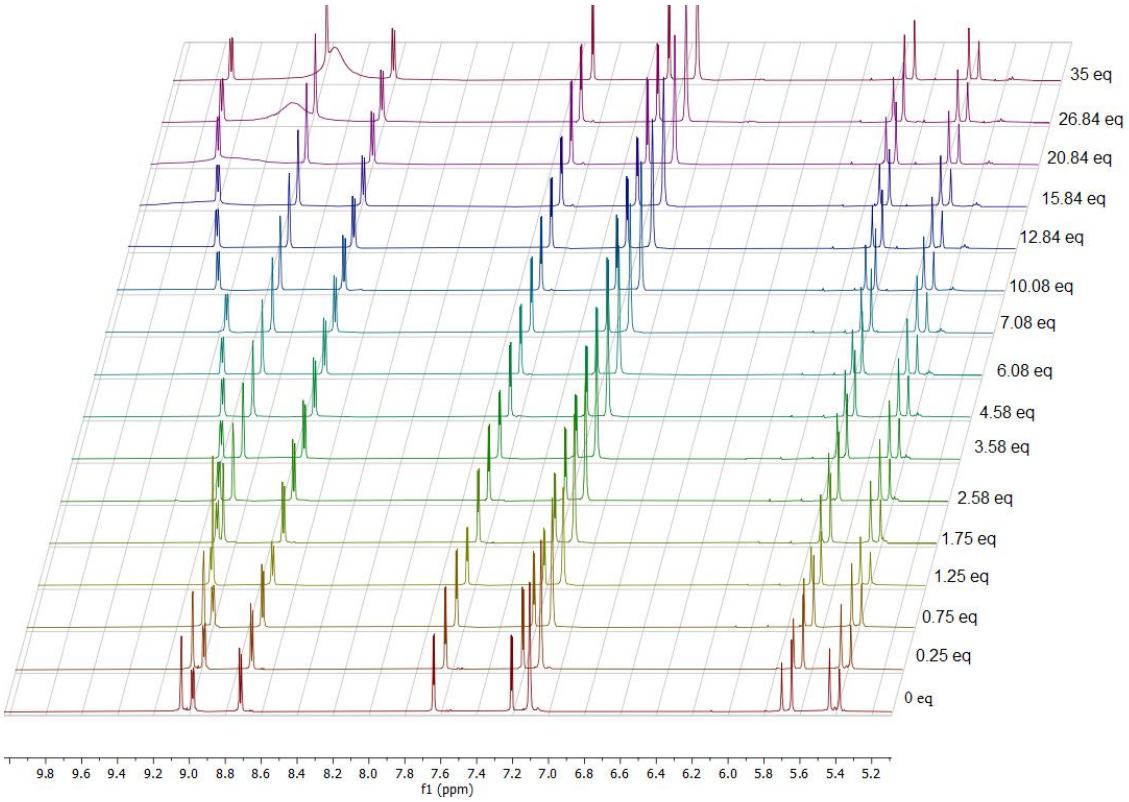

Figure S44. ^{1}H-NMR spectra stacking of **4·PF$_6$** upon successive additions of B(Ar^F)$_3$ in CD_3CN at 298 K.

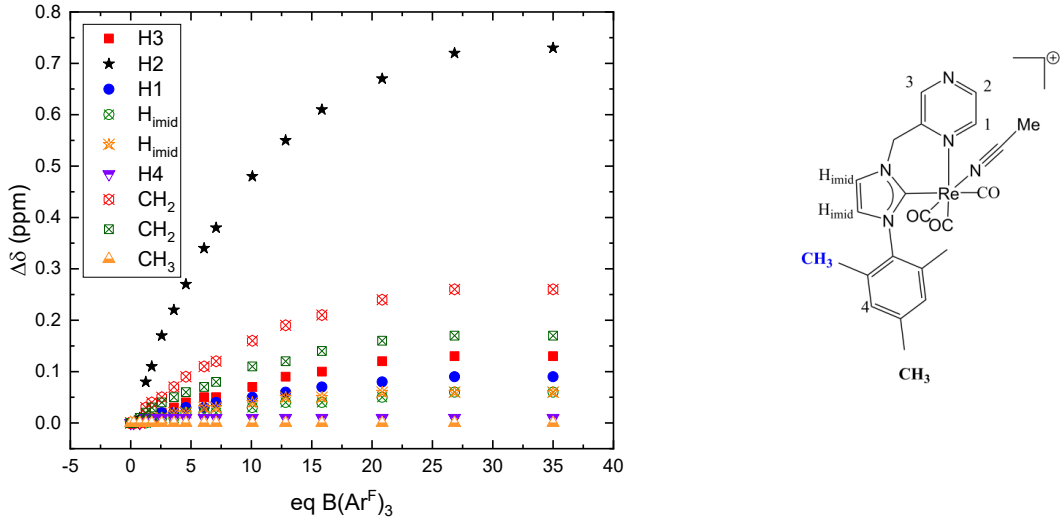

Figure S45. Chemical shifts differences (Δδ) of selected protons at ^{1}H-NMR spectra of **4·PF$_6$** upon successive additions of B(Ar^F)$_3$ in CD_3CN at 298 K.

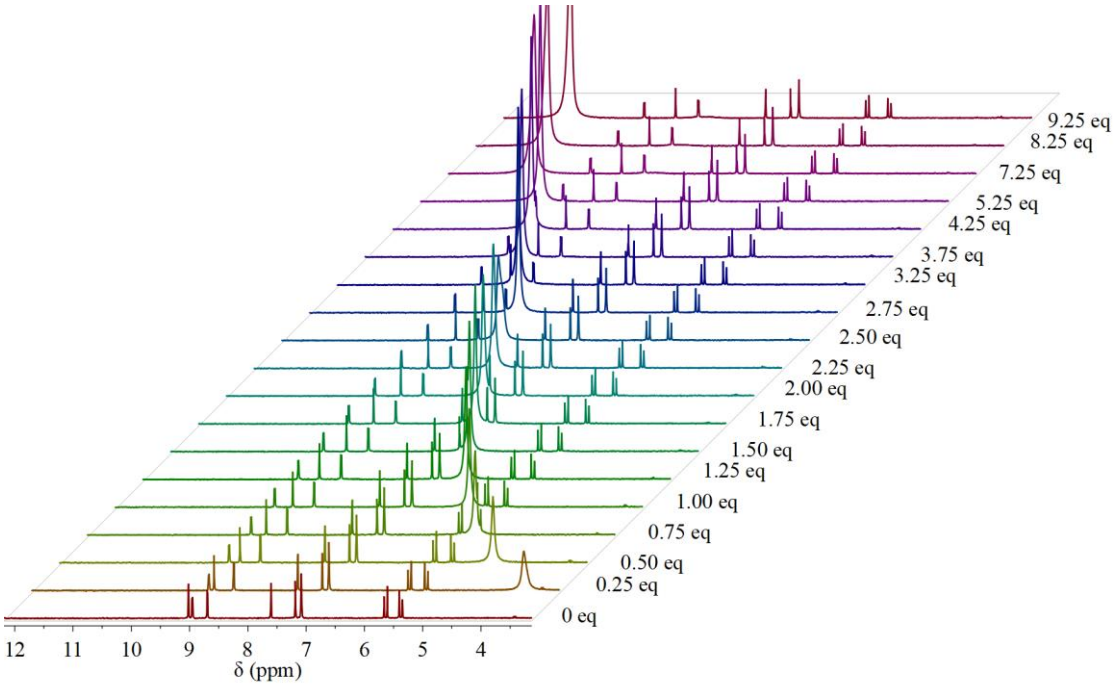

Figure S46. ^{1}H-NMR spectra stacking of **4·PF$_6$** upon successive additions of TfOH in CD_3CN at 298 K.

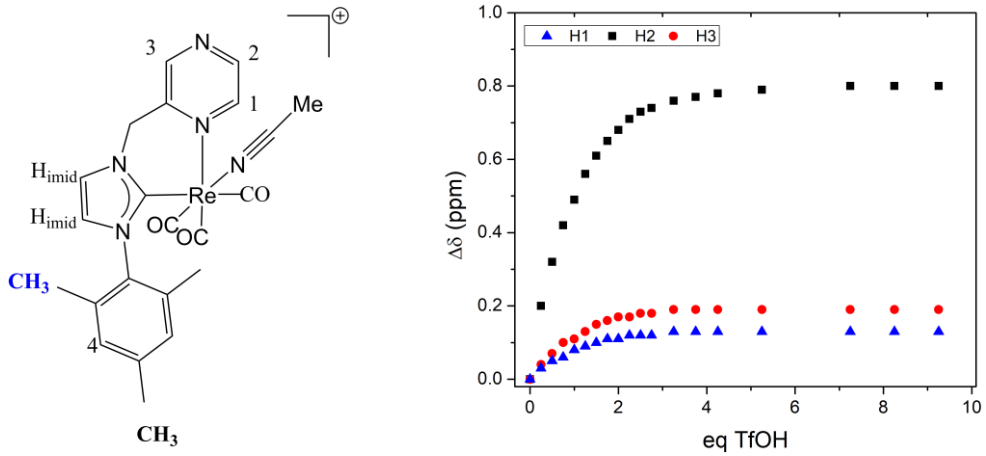

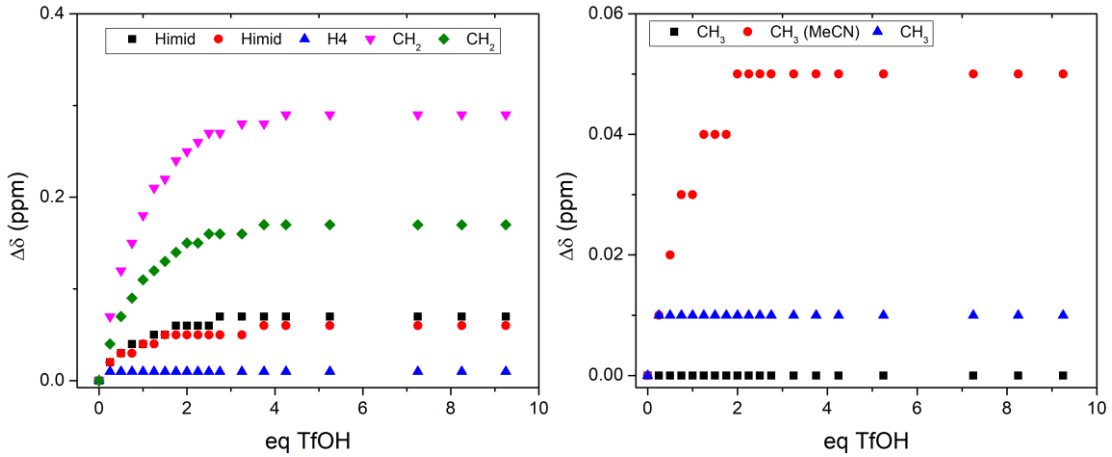

Figure S47. Chemical shifts differences (Δδ) of selected protons at ^{1}H-NMR spectra of **4·PF$_6$** upon successive additions of TfOH in CD_3CN at 298 K.

- Experimental determination of the equilibrium constant by use of NMR chemical shifts

Considering the protonation reaction of complex **4·PF$_6$**, expressed here as "Repz", with TfOH:

$Repz + H^+ \leftrightarrow RepzH^+$
(Reaction 1)

$$K_{eq} = \frac{[RepzH^+]}{[Repz][H^+]} \quad (1)$$

$$[RepzH^+] = K_{eq}[Repz][H^+] \quad (2)$$

Molar fraction: $$\chi_{RepzH} = \frac{[RepzH^+]}{[Repz]+[RepzH^+]} \quad (3)$$

$$\chi_{RepzH} = \frac{K_{eq}[Repz][H^+]}{[Repz]+K_{eq}[Repz][H^+]} = \frac{K_{eq}\cancel{[Repz]}[H^+]}{\cancel{[Repz]}+K_{eq}\cancel{[Repz]}[H^+]} \quad (4)$$

$$\chi_{RepzH} = \frac{K_{eq}[H^+]}{1+K_{eq}[H^+]} \quad (5)$$

Alternatively,[9] the molar fraction of **4·PF$_6$** (Repz) and its protonated form ($RepzH^+$) can be expressed as:

$$\chi_{RepzH} = \frac{\delta_{obs}-\delta_1}{\delta_2-\delta_1} \qquad \chi_{Repz} = \frac{\delta_1-\delta_{obs}}{\delta_2-\delta_1} \quad (6)$$

δ_{obs} = chemical shift observed

[9] a) C. S, Handloser, M. R. Chakrabarty, M. W. Mosher, *J. Chem. Educ.* **1973**, *50*, 510; b) M. A. Swartz, P. J. Tubergen, C. D. Tatko, R A. Baker, *J. Chem. Educ.* **2012**, *89*, 1458–1460.

δ_1 = chemical shift in the absence of protons
δ_2 = chemical shift in the absence of fully protonated species

Thus, representation of χ_{RepzH} vs [H^+] and using equation (5), considering the chemical shift assigned to H2 in the figure below, a K_{eq} = 409 M^{-1} it is obtained.
.

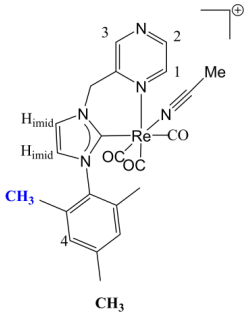

Table S19. Experimental results obtained from titrating complex **4·PF$_6$** with TfOHThe chemical shifts correspond to the H-atom assigned as 2 in the Figure.

[HOTf]	χ_{RepzH}	δ	δ_1	δ_2
0	0	8.95	8.95	9.75
0.00134779	0.25	9.15	8.95	9.75
0.00264323	0.4	9.27	8.95	9.75
0.00392672	0.4375	9.3	8.95	9.75
0.00518577	0.525	9.37	8.95	9.75
0.00642105	0.7	9.51	8.95	9.75
0.00763325	0.7625	9.56	8.95	9.75
0.008823	0.8125	9.6	8.95	9.75
0.00999093	0.85	9.63	8.95	9.75
0.01113761	0.8875	9.66	8.95	9.75
0.01226364	0.9125	9.68	8.95	9.75
0.01325124	0.925	9.69	8.95	9.75
0.0153882	0.95	9.71	8.95	9.75
0.0174521	0.9625	9.72	8.95	9.75
0.01912519	0.975	9.73	8.95	9.75
0.0221601	0.9875	9.74	8.95	9.75
0.02968169	1	9.75	8.95	9.75
0.03278956	1	9.75	8.95	9.75
0.0357211	1	9.75	8.95	9.75

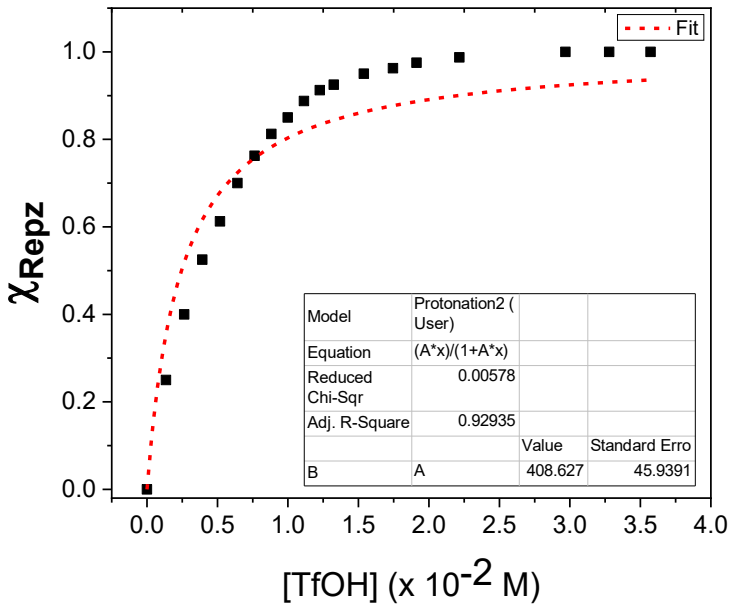

Figure S48. Representation of the molar fraction of the protonation form of **4·PF$_6$** with the concentration of TfOH.

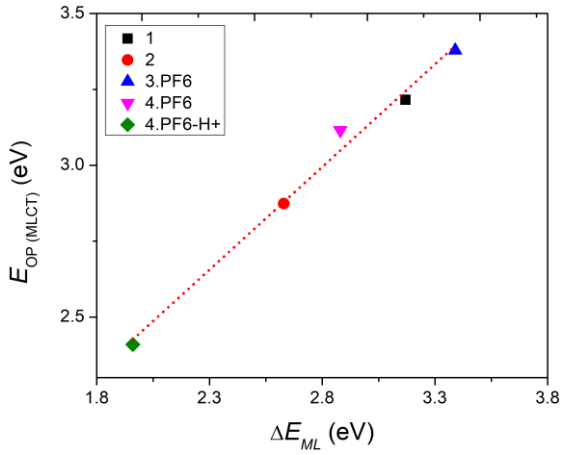

Figure S49. Plot of E_{op} vs ΔE_{ML} in CH_3CN.